Review

Recent Applications and Prospects of Nanowire-Based Biosensors

Vy Anh Tran [1,2,*] , **Giang N. L. Vo** [3] , **Thu-Thao Thi Vo** [4] , **Van Dat Doan** [5] , **Vien Vo** [6] and **Van Thuan Le** [7,8,*]

1. Institute of Applied Technology and Sustainable Development, Nguyen Tat Thanh University, Ho Chi Minh City 700000, Vietnam
2. Faculty of Environmental and Food Engineering, Nguyen Tat Thanh University, Ho Chi Minh City 700000, Vietnam
3. Faculty of Pharmacy, University of Medicine and Pharmacy at Ho Chi Minh City, Ho Chi Minh City 700000, Vietnam; vongoclinhgiang@uphcm.edu.vn
4. Department of Food Science and Biotechnology, Gachon University, 1342 Seongnamdaero, Sujeong-gu, Seongnam-si 13120, Republic of Korea; vothuthaobd@gmail.com
5. The Faculty of Chemical Engineering, Industrial University of Ho Chi Minh City, Ho Chi Minh City 700000, Vietnam; doanvandat@iuh.edu.vn
6. Faculty of Natural Sciences, Quy Nhon University, 170 An Duong Vuong, Quy Nhon, Binh Dinh 55000, Vietnam; vovien@qnu.edu.vn
7. Center for Advanced Chemistry, Institute of Research and Development, Duy Tan University, 03 Quang Trung, Da Nang 550000, Vietnam
8. Faculty of Natural Sciences, Duy Tan University, 03 Quang Trung, Da Nang 550000, Vietnam
* Correspondence: tavy@ntt.edu.vn (V.A.T.); levanthuan3@duytan.edu.vn (V.T.L.)

Abstract: High-sensitivity biomedical sensors could make it possible to detect and classify chemical and biological species in a variety of applications, from disease diagnosis to medication discovery, thus, boosting the likelihood of life-saving intervention. Synthesized nanowires have already produced advancements in a variety of sectors, including biological sensors over the last decade. When compared to macro-sized materials, the nanowires' large surface area-to-volume ratio increased sensitivity. Their applications for biomarker, viral, and DNA detection, as well as drug discovery, are also discussed. Self-powering, reusability, sensitivity in high ionic strength solvents, and long-term stability are all examples of recent developments. Shortly, the nanowire is likely to lead to major improvements in biomedical sensors. This review provides a full overview of the nanowire sensor's working principle and production procedure. We have discussed how to produce nanowires that can be utilized as biosensors for different bacteria and pathogens, protease, DNA and RNA, neurotransmitters, and chemical compounds. Biosensing technology has dramatically improved because of the introduction of nanowires in biosensors. This is a result of the application of new biorecognition components and transducers, improvements in the manufacture, design, and miniaturization of nanostructured devices at the micron scale, and unique approaches for the synthesis of nanowires. The versatility, robustness, and dynamic nature of sensing technologies have all improved thanks to the usage of nanowires.

Keywords: nanowires; biological sensors; neurotransmitter detection; DNA/RNA detection; viral detection; protein detection

1. Introduction

Structures with a thickness or diameter limited to tens of nanometers or less and an unrestricted length are known as nanowires. The phrase "quantum wires" originated from the importance of quantum mechanical effects at these scales. There are several different kinds of nanowires, including superconducting, metallic (Au, Ag, Ni, and Pt) [1–4], semi-conducting, and insulating ones (TiO_2, SiO_2) [5]. Recent research has shown that nanowires can be used as basic tools to create nanoscale probes for a variety of purposes, including biosensing, electrophysiology, intracellular matter transfer, mechanical transduction, and

immunomodulation [6,7]. The optical performance, electrical characteristics, chemical composition, and topographies are only a few of the highly modifiable parameters that may be found in nanowires. Different surface functionalization on various nanowires can be used to achieve a variety of biochemical sensing approaches, considerably expanding the applications for chemical and biomolecular (H_2O_2, nucleic acids, glucose, and proteins) sensing [5,8,9].

Several cells can be sensed using nanowires in a high-throughput, high-spatiotemporal-resolution manner [10]. Nanowire can be used for analyzing extracellular biophysical signals, such as the contraction force and mechanical transduction of cells, in addition to biomolecular sensing [11,12]. Significantly, devices that sense and stimulate cells have been produced using nanowire-based sensing platforms. They might offer opportunities to simultaneously detect a variety of biological substances [13,14]. Nanowires provide for the least intrusive operation of cells due to their high controllability and excellent biocompatibility [15,16]. The usage of patterned nanowires could help with the difficult task of detecting more intracellular signals as well as the collection of long-term, high-throughput signals. The high specific surface area of nanowires, which offers a large number of attaching sites for detecting receptors, biomarker molecules, or cells, contributes to their great sensitivity [17,18]. Yet, the 3D sensing matrix also ensures multichannel detection of weak or spatially dependent bio-signals [19,20]. On the other hand, the meticulous shape and multi-level structure that enables easy attachment to particular cell structures like tentacles and synapses should partially account for the great selectivity of nanowires. The adaptable bio-recognition layer also offers a synergistic contribution to the controllable selectivity of nanowires [21,22].

The discovery and diagnosis of disease, as well as the development and screening of new therapeutic compounds, are all areas of healthcare and the life sciences where the detection of biological and chemical species is crucial [23–25]. Therefore, the creation of new tools that allow for a quick, sensitive, and direct examination of these species has the potential to have a big impact on humanity [26–28]. Nanowire-based devices are becoming a potent and versatile class of electrical sensors with extreme sensitivity for the direct detection of biological and chemical species [5,29,30]. To identify, prevent, and cure illness, biosensors have been crucial in the development of testing kits, vaccinations, and antiviral medications. Because they have several benefits, including quick and continuous measurement, high sensitivity and low specificity, and the use of fewer reagents, they have been widely used as immuno-sensors for the detection of target biomolecules in bodily fluids [31]. Yet, in a clinical therapy, the biosensor's detection limit cannot be sufficient. The sensitivity of sensors can be affected by the extremely low possibility of false-positive results in the low concentration range. Thus, it is essential to create a highly sensitive sensor system with a wide dynamic range to find clinically significant indicators [29].

This review emphasizes recent developments in biosensors based on nanowires. We briefly describe the creation of efficient sensing methods that use biosensors built on nanowires, such as Ribonucleic Acid (RNA), (Deoxyribonucleic Acid) (DNA), proteins, neurotransmitters, and viruses. Moreover, this review offers a thorough grasp of the design methods and corresponding methodologies for nanowire-based biosensors used for distinct biomedical sensing activities. In contrast to publications that concentrate on a single application area or type of nanowire material, this study examines a variety of biosensing applications and nanowire materials. Lastly, the prospects of useful biomedical platforms are examined with a focus on the development and application directions of nanowire-based biosensor arrays.

2. Fabrication Process and Working Principle of Nanowire

2.1. Fundamentals of Nanowire Fabrication Process

Nanowire synthesis can be carried out in one of two ways: top-down or bottom-up. A top-down strategy uses techniques such as lithography, milling, or thermal oxidation to break up large chunks of material into smaller ones. A bottom-up strategy is used to

combine adatoms to create the nanowire. The majority of synthesis methods take a bottom-up strategy. To fine-tune the size and aspect ratio of the structures, initial synthesis using either method may frequently be followed by a nanowire heat treatment phase. This stage frequently involves a type of self-limiting oxidation (Figure 1). Suspension, electrochemical deposition, and vapor deposition are three prominent ways to construct nanowires [32].
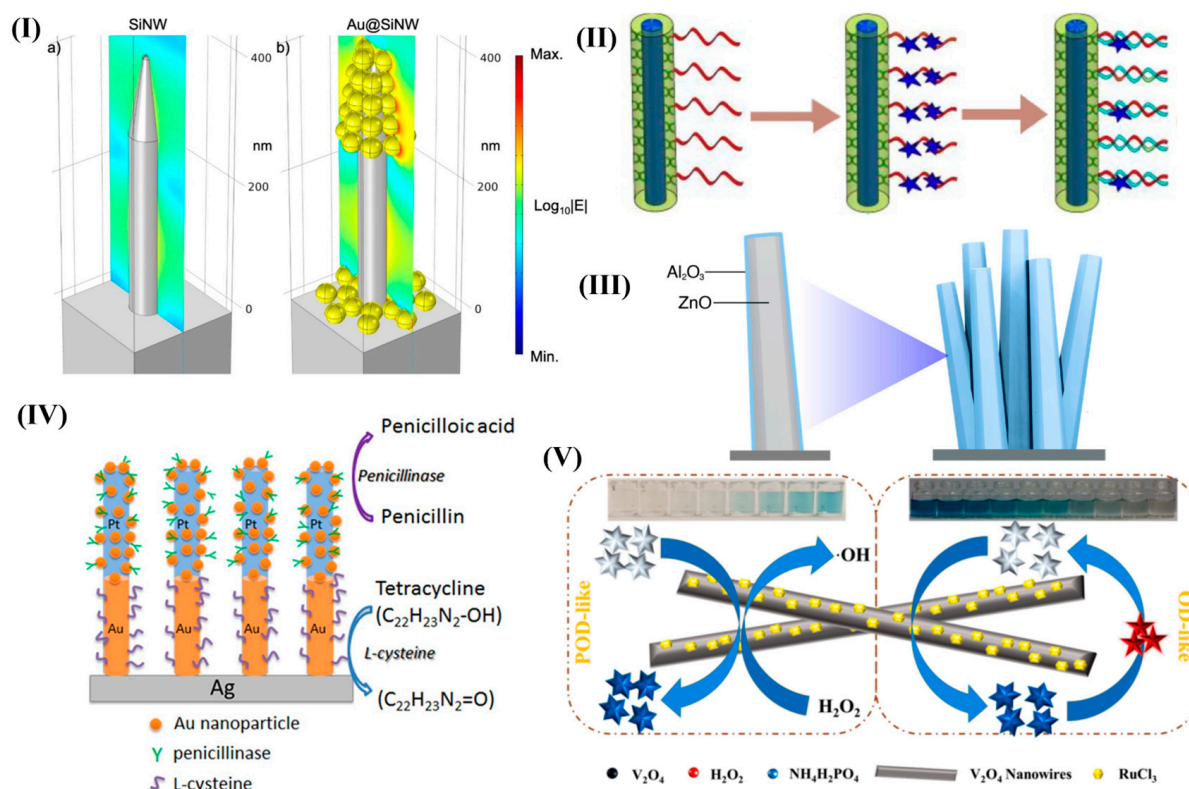

Figure 1. A typical synthesis of nanowires applied in biosensors including (**Ia,Ib**) Au@SiNW substrate; (**II**) PEG/PPy nanowires; (**III**) schematic illustrations of ZnO/Al$_2$O$_3$ core–shell nanowire; (**IV**) the Au–Pt multi-segment nanowire array; and (**V**) Ru@V$_2$O$_4$ nanowires for sensitive colorimetric H$_2$O$_2$ and cysteine sensing. Reproduced with permission from [33–37]. Copyright 2021, 2019, 2019, and 2021 ACS, Elsevier, Elsevier, and Elsevier.

There are other additional techniques for synthesizing nanowires that are being carefully studied, developed, and used for biosensor applications:

Electrospinning: The process of electrospinning uses an electric field to spin nanofibers from a polymer solution. The threads are then gathered to create a network of nanowires on a substrate.

Template-assisted synthesis: Using a template to direct the formation of nanowires is known as "template-assisted synthesis." A self-assembling monolayer or a porous membrane can serve as the template.

Vapor–liquid–solid (VLS) growth: In this technique, nanowires are grown from a vapor-phase precursor using a metal catalyst.

2.2. Working Principle of Nanowire for Biosensor

To provide a quantifiable signal, a biosensor combines a transducer with a biological element, such as an enzyme or antibody. The transducer detects, records, and transmits data regarding a physiological change or the presence of various chemical or biological elements in the environment. The sizes and designs of biosensors vary, and they may monitor and detect even extremely minute amounts of some diseases, dangerous chemicals, and pH levels [38].

A basic biosensor consists of: (i) either a biomolecule or biological element that may recognize the target substrate (glucose, lactose, enzymes, DNA, RNA, or virus), or an analyte, which is a material of interest whose contents are being identified or detected. (ii) A transducer that transforms energy from one form into another. The transducer is an essential part of a biosensor. The biorecognition event is converted into an electrical signal that can be monitored and connected to a target that is chemical or biological, as well as a quantity. (iii) The transduced signal is processed and made ready for display in step. Electrical signals from the transducer are amplified and converted into digital signals. The processed signals are quantized using the display unit. According to the analyte, or signal detection to be monitored, biosensors can generally be categorized into a variety of categories [39].

3. Application of Nanowire for Biosensor

3.1. Detection of Various Neurotransmitters and Molecular

Biological molecules such as nucleic acids, neurotransmitters, and small molecules can currently be recognized. The operation of a biosensor is based on the interaction of the target analyte and biological recognition component. When the target analyte connects to the biological recognition element, it emits a signal, which the transducer then turns into an electrical signal. Several industries, including environmental monitoring, food safety, and medical diagnostics, use these biosensors. Dopamine, as well as glucose, cholesterol, and other chemicals can be selectively detected using biosensors (Table 1).

Table 1. Characteristics of nanowire systems for neurotransmitter and molecular detection.

Materials	Mechanism	Target	Concentration Range	Limit of Detectiozn	Ref.
Silicon NWs	Fluorescent signal	γ-Aminobutyric acid (GABA)	970 fM to 9.7 μM	9.7 μM	[40]
Pt-Au NWs	Cyclic voltammetry (CV)	Penicillin and tetracycline	300–240 μM 300–210 μM	41.2 μA μM^{-1} cm^{-2}, 26.4 μA μM^{-1} cm^{-2}	[36]
Ru@V$_2$O$_4$ nanowires	Colorimetric sensor	Cysteine	3–50 μM	0.139 μM	[37]
Cu$_2$O/Cu@C core–shell NWs	Amperometry	Uric acid	0.05 to 1.15 mM	330.5 μA·mM^{-1}·cm^{-2}	[41]
Rutile/anatase TiO$_2$ (R/A-TiO$_2$)	Photoelectrochemical biosensor	Glucose	1–20 mM	0.019 mM	[42]
Mo-W-O NWs intercalated graphene	Electrochemical sensor (CV, Differential pulse voltammetry (DPV))	Dopamine and Tyrosine	0.001–448.0 μM, 0.001–478.0 μM	0.8 nM, 1.4 nM	[43]
CuO/Cu$_2$O NWs	Photoelectrochemical	Tyrosinase	0.05–10 U/mL	0.016 U/mL	[44]

Lee et al. developed an immunosensor based on a silicon nanowire field-effect transistor (FET) device to identify the GABA molecule [40]. By using electron beam lithography, zigzag-shaped silicon nanowires were synthesized, and a semiconductor analyzer was used to verify the p-type FET device's electrical properties. By measuring the fluorescence signal, the ideal immobilizing circumstance for the antibody against the GABA molecule was identified. Using the immunoreactions, the conductance change on silicon nanowire-based devices was sensitively used to quantify different GABA concentrations ranging from 970 fM to 9.7 μM (Figure 2).
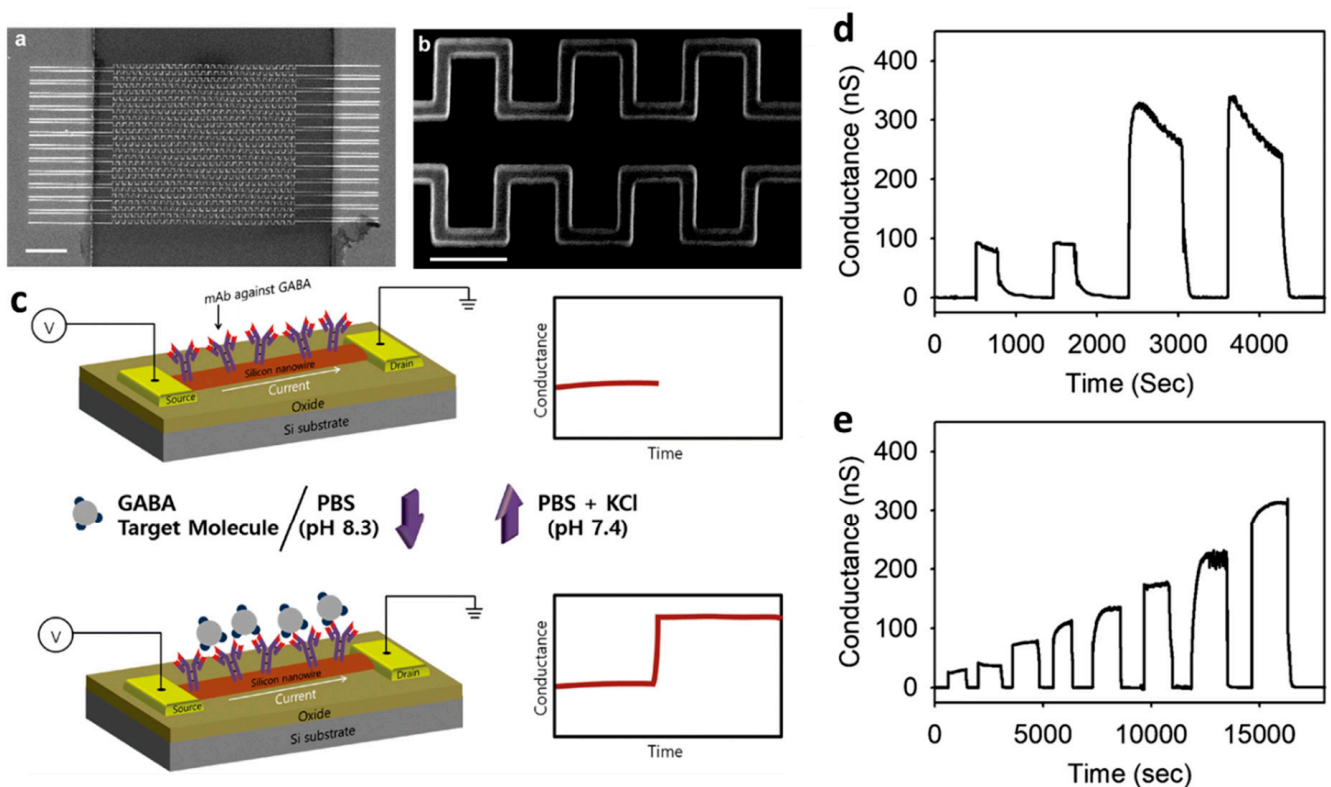
Figure 2. Generated nanowire pattern on SOI wafer as seen in the scanning electron microscope image in (**a**,**b**) device schematic for a field effect transistor based on silicon nanowires to detect GABA (scale bars: 5 m, 500 nm). (**c**) This system's conductance increased when GABA was added as a result of an immunoreaction, which was observed using a FET device based on silicon nanowires. (**d**) A reproducible conductance signal is seen through certain GABA molecule concentrations. (**e**) After using the GABA target molecule, the conductance versus time measurements on the GABA antibody-modified p-type silicon nanowire vary from 970 fM to 9.7 μM. Reproduced with permission from [40]. Copyright 2019 Springer.

For the simultaneous detection of penicillin and tetracycline, a hybrid nanowire/nano-particle array containing a range of bio-molecular sensors was used to build an electrochemical biosensor. The penicillinase was then immobilized on the Au NPs using 1-Ethyl-3-(3-dimethylaminopropyl)carbodiimide/N-hydroxysuccinimide (EDC/NHS) cross-linked after being electroless plated on the Pt nanowire segments using L-cysteine to create a monolayer on the Au segment as the bio-receptor for tetracycline detection. The vertically aligned Pt–Au nanowire array was prepared by an electrodeposition method within the anodic aluminum oxide (Figure 3).The electrode of Au(L-cysteine)–Pt(penicillinase) demonstrated simultaneous detection capability and astonishingly high sensitivities of tetracycline and penicillin, with values of 41.2 A μM^{-1}cm^{-2} (penicillin) and 26.4 A μM^{-1}cm^{-2} (tetracycline). Investigated sensitivities were analyzed with various segment lengths. Tests on actual samples using extracts of chicken and beef produced positive results for recovery [36].
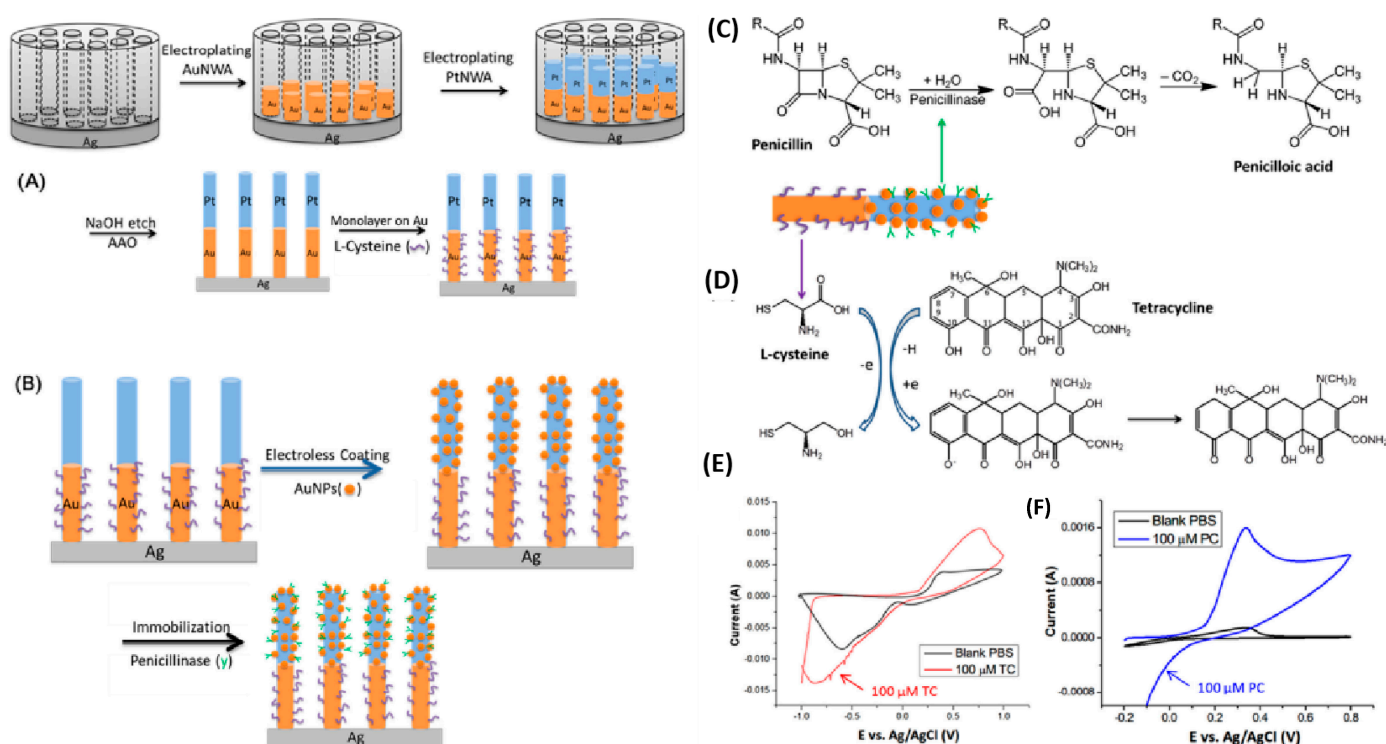
Figure 3. The manufacturing of nanowire of Au–Pt multi−segment assembly: L−cysteine on the Au is shown schematically in (**A**); electroless plating of Au NPs on Pt region followed by the enzyme of penicillinase (**B**); the sensing mechanisms of penicillinase and penicillin (**C**); L−cysteine and tetracycline (**D**). Cyclic voltammetry of the nanowire arrays of (**E**) Au(L−cysteine) sensing 100 μM tetracycline (1 mM PBS) and (**F**) Pt (Penicillinase) detecting 100 μM penicillin (1 mM PBS). Reproduced with permission from [36]. Copyright 2019 Elsevier.

A one-step hydrothermal technique was used to create a Ru@V_2O_4 nanocomposite with enzyme-like activities. The tetra-enzyme-like activities of the produced Ru@V_2O_4 NWs, including peroxidase-like, oxidase−like, superoxide dismutase-like, and catalase−like activity, were developed (Figure 4). The peroxidase-like and oxidase-like behaviors of Ru@V_2O_4 nanowires, which were following the Michaelis–Menten kinetics, were first validated by the kinetic investigation. Next, using Ru@V_2O_4 nanowires' POD− and OD−like enzymatic activity, a polyfunctional colorimetric sensor platform was developed for the detection of cysteine (Cys) and H_2O_2. The response limit for H_2O_2 detection using Ru@V_2O_4 nanowires was 0.788 μM, and the detection range for H_2O_2 was 1–500 μM. In ideal circumstances, the degree of discoloration had a low detection limit of 0.139 μM and was linearly proportional to the Cys concentration in the range of 3–50 μM. Moreover, Ru@V_2O_4 nanowires can identify Cys in serum and H_2O_2 in samples collected [37].

Thermal degradation of [Cu_3(btc)$_2$(H_2O)$_3$] MOF (HKUST-1) NWs results in the synthesis of porous Cu_2O/Cu@C core–shell nanowires. The NWs are subsequently employed as materials for electrodes to create Uric Acid (UA) sensors (Figure 5). By manipulating the calcination settings, authors can create composite NPs made of copper NPs and cuprous oxide that are encased in a non-graphitic carbon nanowire shell. These NWs have strong electrocatalytic performance at low working voltage, which helps UA biosensors become more interference resistant. The substrate's copper and carbon content also speed up electron transfer, which significantly raises the UA biosensors' sensitivity. At a working potential of −0.5 V versus SCE, a sensitivity of 330.5 μAmM^{-1}cm^{-2} and a linearity range of 0.05–1.15 mM are attained [41].
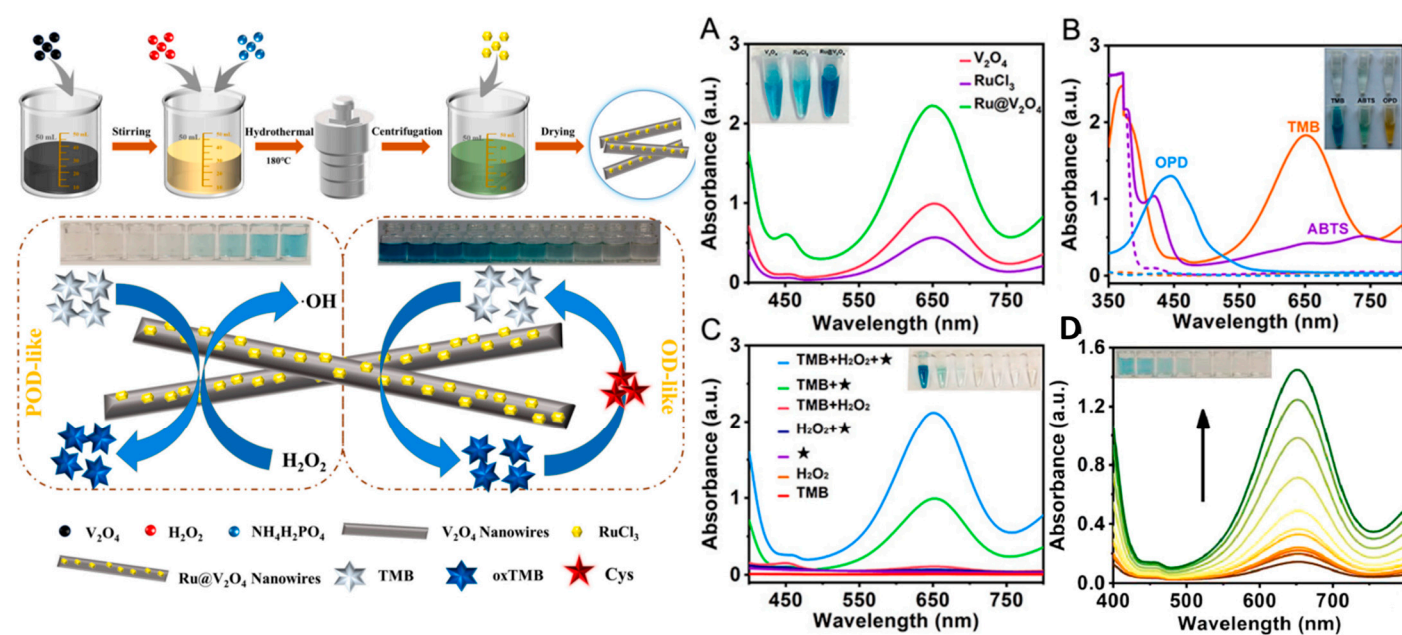
Figure 4. The synthesis of Ru@V_2O_4 NWs with good tetra-enzyme and the colorimetric sensor method for Cys and H_2O_2 are shown schematically (left image). The activity of catalysis of three distinct substances (RuCl$_3$, V_2O_4 NWs, and Ru@V_2O_4 NWs) on TMB is shown in (**A**). (**B**) Spectra of UV-vis absorption of reactions catalyzed using Ru@V_2O_4 NWs, including OPD (blue line), ABTS (purple line), and TMB (yellow line). Individual ABTS, TMB, or OPD are shown by the accompanying dashed lines. Spectra of TMB, H_2O, Ru@V_2O_4 nanowires, Ru@V_2O_4 nanowires/TMB/H_2O_2, Ru@V_2O_4 nanowires/TMB, TMB/H_2O_2, and Ru@V_2O_4 nanowires/H_2O_2, are shown in (**C,D**). Reproduced with permission from [37]. Copyright 2021 Elsevier.

3.2. Detection of DNA and RNA

The research of DNA and RNA detection methods has received significant interest due to its wide range of potential applications, including the identification of clinical diagnoses, the recognition of DNA-based gene sequences, nano-bioengineering, and the field of food science [45]; many approaches, including electrochemical [46], optical fiber sensors [47], and surface plasmon resonance biosensors techniques [48], have been thoroughly studied for DNA sensor (Table 2). Scientists' ability to successfully diagnose pathologies is especially important for success in the field of healthcare science [49].

Shariati has developed a label-free, field-effect transistor DNA sensor for the hepatitis B virus (HBV) using indium tin oxide (ITO NWs) [49]. ITO nanowires' robust conductance and functionally changed surface led to an increase in probe immobilization and target hybridization. ITO NWs had a diameter of less than 50 nm of crystalline, according to a measurement made using HRTEM. On the Au-modified nanowires, the single-stranded hepatitis B virus DNA (SS-DNA) was immobilized as a probe. The linear concentration range of the DNA targets was 1 fM to 10 μM. The DNA biosensor has a limit of detection (1fM). For a specific single strand, the hybridization process took 90 min. The biosensor had a 1.1×10^5 switching ratio between the on and off states. DNA oligonucleotide sequences that belong to mismatched, complementary, and non-complementary were readily distinguishable for biosensor sensitivity. The highly satisfying specificity for distinguishing complementary sequences from non-complementary and mismatched oligonucleotides was proven using the HBV sensor (Figure 6).
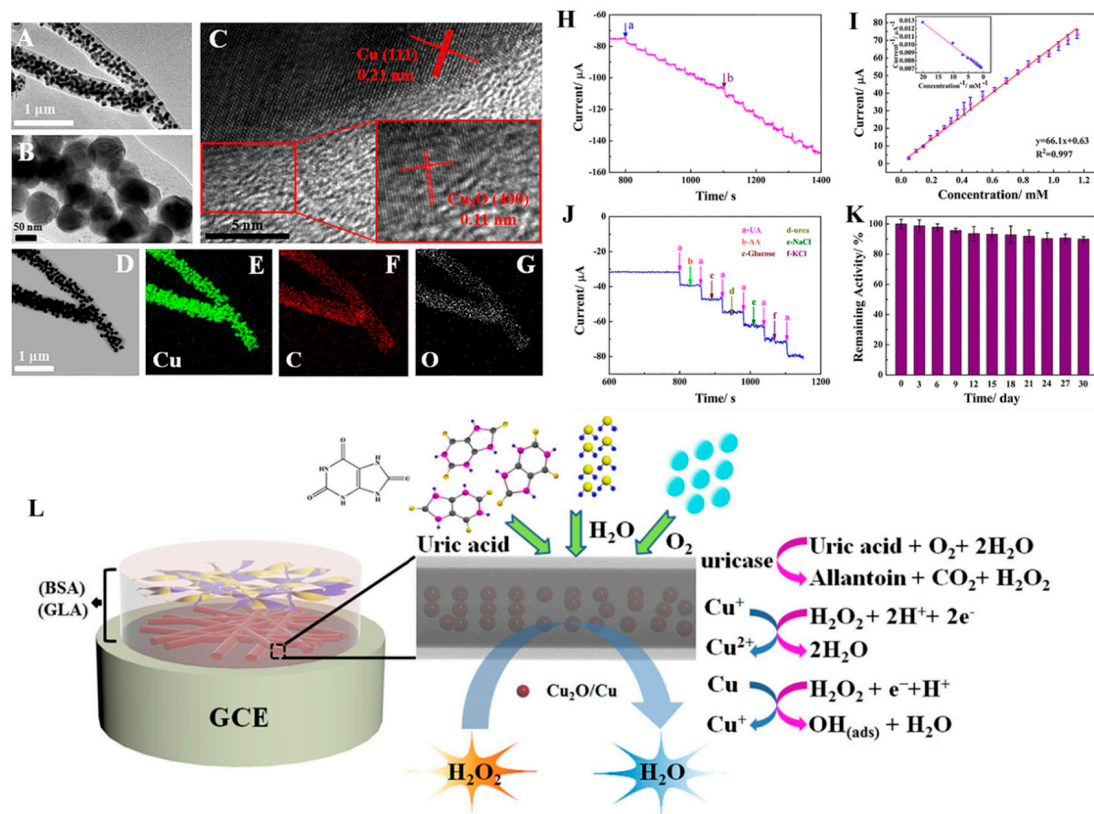
Figure 5. Core–shell $Cu_2O/Cu@C$ NWs are shown in: (**A,B**) TEM images, (**C**) HRTEM images, (**D–G**) images of EDX mapping, and (**H**) the amperometric responses of UA sensors using core–shell $Cu_2O/Cu@C$ NWs with the serial injection of UA at various concentrations. (**K**) Selectivity of as-prepared UA sensors and (**L**) The stability of UA sensors after 1 month. Sensor mechanism of the UA sensors using core−shell $Cu_2O/Cu@C$ NWs: 0.05 mM (**I**) and 0.1 mM (**J**) standard curve of it as UA sensors. Reproduced with permission from [41]. Copyright 2020 Elsevier.

Table 2. Characteristics of NWs biosensor for DNA/RNA detection [5].

| Materials	Mechanism	Target	Concentration Range	Limit of Detection	Ref.
ITO NWs	FET	DNA of hepatitis B virus (HBV)	1 fM to 10 µM	1 fM	[49]
Core D-Shaped Photonic Crystal Fibre Embedded silver nanowires	Surface Plasmon Resonance	DNA/RNA	1.35 to 1.50 RIU	4000 nm/RIU	[35]
Silicon NWs	FETs	Hepatitis C virus (nDNA)	10–328 mM	10 mM	[50]
TiO_2 NWs	fluorescence	ssDNA; dsDNA;	2 nM to 200 nM	1.4 nM	[51]
SOI NWs Chip	Micro-Raman	Circular RNA (Glioma)	10^{-16}–1.1×10^{-16} M	10^{-16} M	[52]
(PEG)-polypyrrole (PPy) nanowire	Differential pulse voltammetry (DPV)	miRNA	0.10 pM ~ 1.0 nM	0.10 pM	[34]
SiNWFETs/PEG-mSAMs	FETs	miRNA-21	10 aM–10 pM	10 aM	[53]
Morpholino-functionalized Si NWs	Label-free detection	DNA	1 nM–100 pM	100 pM	[54]
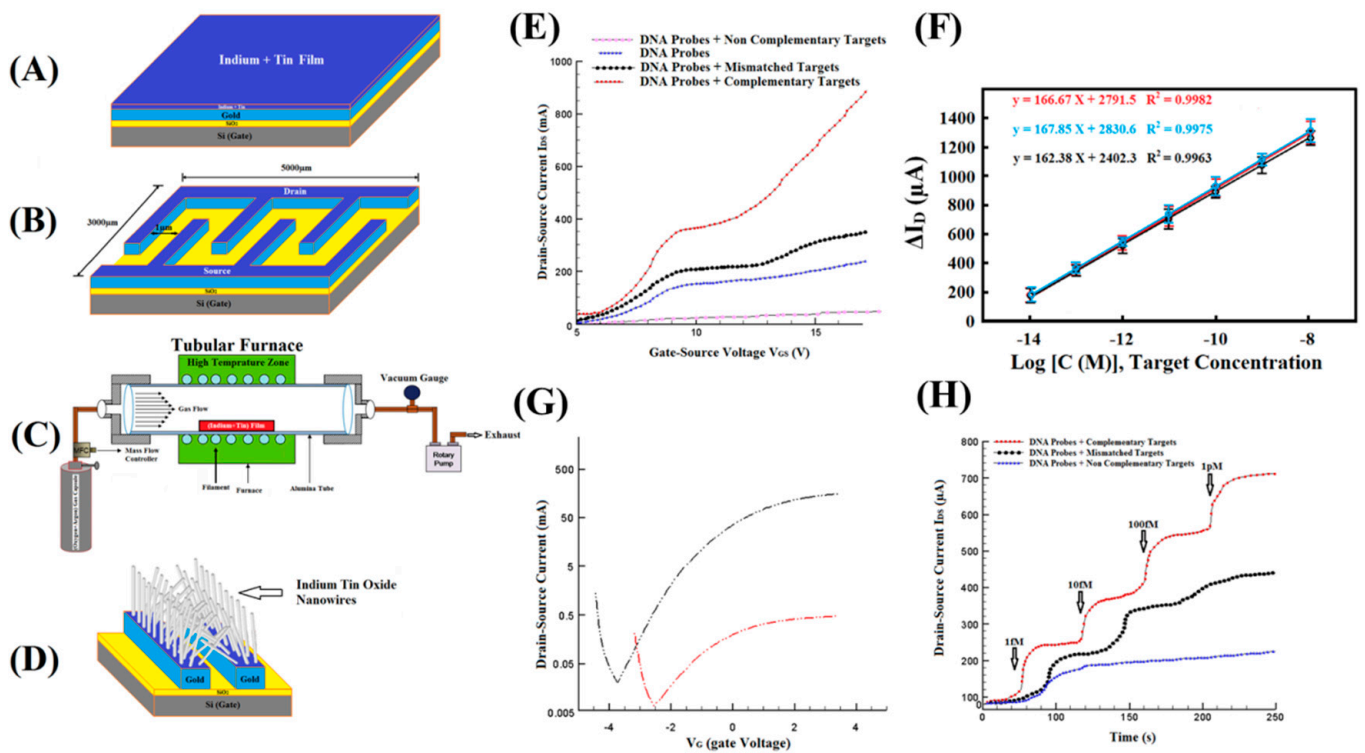
Figure 6. The development of a FET device using ITO nanowires. (**A**) The gold film was covered with an indium and tin film. The P-Type semiconductor that serves as the back-gate electrode is the Si platform (SiO_2 layer). (**B**) E-beam lithography was used to form the electrodes and FET design. (**C**) A diagram of a tubular furnace. (**D**) The under-controlled production of NWs in a tube furnace. (**E**) IDS–VGS graphs from a synthesized transistor of ITO NWs after immobilizing probes; VDS was set to a value of +3 V. (**F**) The transfer properties were toggled from on to off before hybridization (red curve) and after (black curve), with VDS = +3 V. The lowest limit of detection was 1 fM in (**G**) the link between current changes and concentration. Regarding the DNA biosensor's consistency and repeatability across three (blue line) and five weeks (black line); after three and five weeks, respectively, it reached 98% and 96% of its initial response. The dynamic evaluations of the FET biosensor. (**H**) The sensor's dynamic tests use mismatched, non-complimentary, and complementary targets. At VDS = +1 V and VGS = +2 V, the ITO NWs reaction and expected outputs were obtained. Reproduced with permission from [49]. Copyright 2018 Elsevier.

The annealed ZnO/Al_2O_3 core–shell nanowire device was developed by Hiromi et al. as a platform for RNA capture (Figure 7). Comparing the efficiency of capturing RNAs to that of other circulating nucleic acids, such as genomic DNA (gDNA) and cell-free DNA (cfDNA), the annealed ZnO/Al_2O_3 core–shell nanowire could capture RNAs with a high level of efficiency. Moreover, the Al_2O_3 shell's crystalline structure, which acts as a protective layer to stop nanowire degradation, was thought to make the nanowire biocompatible with blood plasma samples. Potentially serving as a platform for RNA-based extraction and detection, the devise was developed [35].
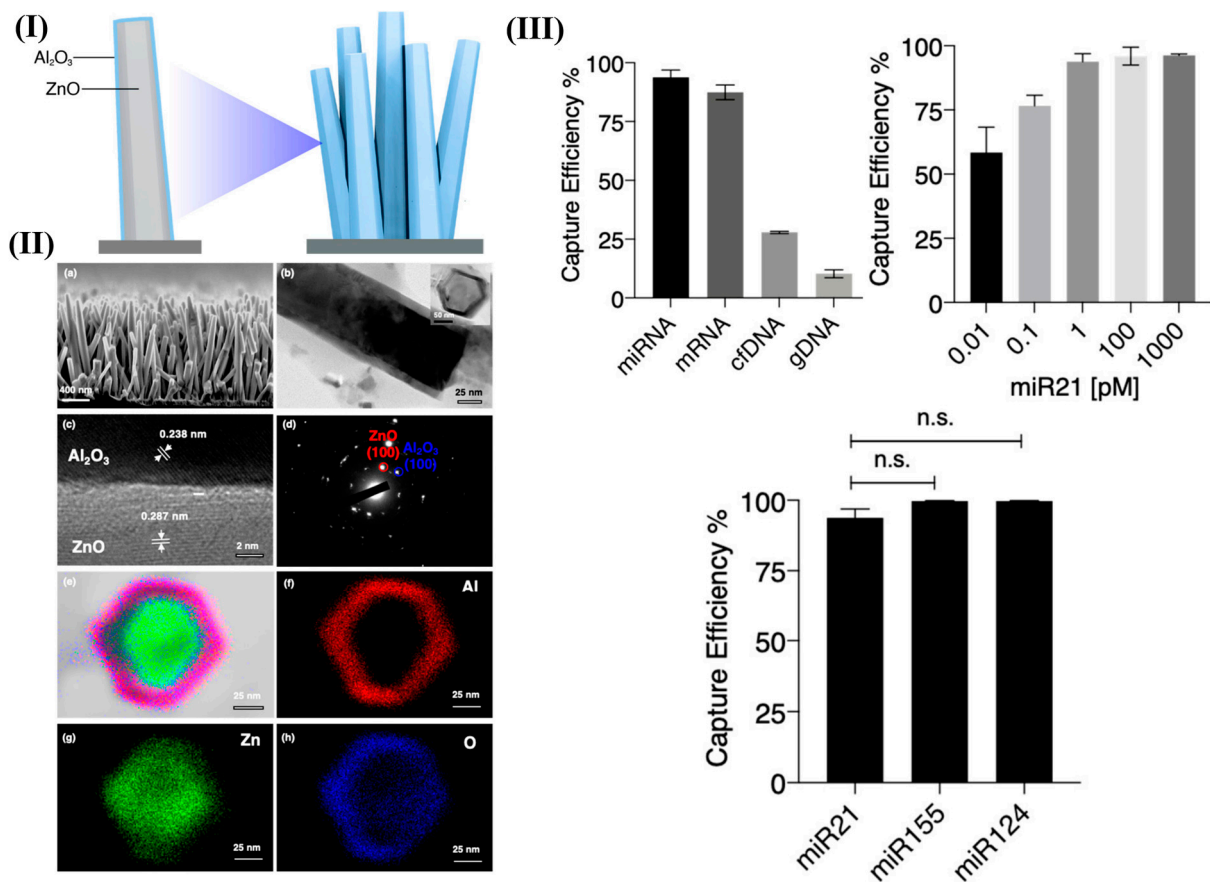
Figure 7. (**I**) ZnO/Al$_2$O$_3$ core–shell nanowire schematic illustrations; (**II(a–h)**) SEM and TEM images of the nanowire—atomic-resolution TEM images of the nanowire showing orientation growth of (100) ZnO and (110) Al$_2$O$_3$; and (**III**) Capture of miRNAs on annealed ZnO/Al$_2$O$_3$ core–shell nanowires, comparison of the nucleic acids', miRNAs', mRNAs', cfDNAs', and gDNAs' capture efficiency. Capture efficiency of miR21 on nanowire at concentrations of 0.01, 1, 10, and 1000 pM; comparison of miR21, miR155, and miR124 capture efficiencies. Error bars for a set of measurements (n = 3) display the standard deviation. Reproduced with permission from [35].

To provide superior antifouling performances, Wang et al. have developed ultrasensitive sensors based on polyethylene glycol-polypyrrole ((PEG-PPy) NWs [34]. Using electrochemically polymerizing pyrrole at the constant voltage on the glassy carbon electrode (GCE), PPy nanowire arrays were manufactured. By electrochemically oxidizing the amine groups provided by the PEG end chains, the surfaces of PPy nanowires were embellished with 4-armed PEG molecules. The highly effective antifouling qualities of PEG and the exceptional electrical conductivity of PPy nanowires, a conducting polymer, are synthesized in the newly developed PEG/PPy nanowires. MicroRNAs (miRNAs) are potential indicators of the onset, prognosis, and risk of diseases because they play critical roles in the development of cancer and several other diseases. It is simple to create an ultrasensitive electrochemical biosensor for miRNA by immobilizing DNA probes on PEG/PPy NWs. Changes in the methylene blue (MB) redox signal were tracked using the differential pulse voltammetry method to measure DNA/RNA hybridization. The biosensor produced a large linear range (0.10 pM–1.0 nM) to the target miRNA, and miRNA mismatches can also be satisfactorily discovered with ease (Figure 8).
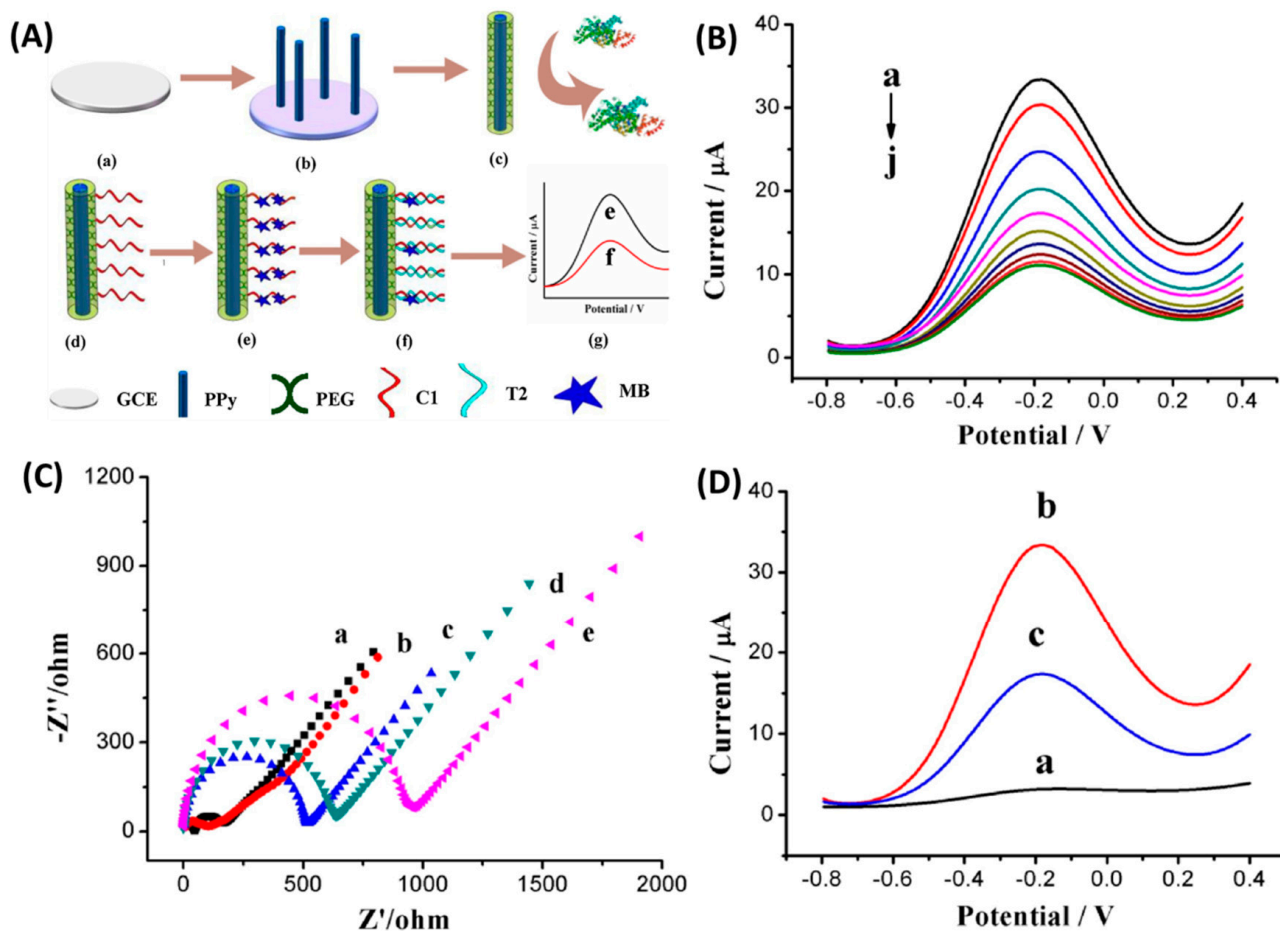
Figure 8. (**A**(**a**–**g**)) Diagrammatic representation of the improved sensor manufacture using PEG/PPy NWs and antifouling properties. A plain GCE, PPy/GCE, aPEG/PPy/GCE, C1/PEG/GCE, MB/C1/PEG/GCE, T2/MB/C1/PEG/GCE, and DPV result are examples of outcomes. (a) bare GCE (b) PPy/GCE (c) PEG/PPy/GCE (d) C1/PEG/GCE (e) MB/C1/PEG/GCE (f) T2/MB/C1/PEG/GCE (f) DPV results (**B**) Common DPV spectra for the incubation of MB/C1/PEG/PPy/GCE with various target miRNA concentrations (10^{-15} M–10^{-7} M) are shown in order from top to bottom. (**C**) Electrochemical Impedance Spectroscopy (EIS) data were captured at the following locations: GCE (a); PPy/GCE (b); PEG/PPy/GCE (c); C1/PEG/PPy/GCE (d); and T2/C1/PEG/PPy/GCE (e). DPV characterization of MB/C1/PEG/PPy/GCE recorded before (curve b) and after (curve c) target miRNA (T2) hybridization is shown in (**D**) together with the C1/PEG/PPy/GCE DPV curve (black line a). Reproduced with permission from [34]. Copyright 2019 Elsevier.

3.3. Detection of Protein

To identify certain proteins in biological samples, biosensors for protein detection are used. An enzyme, protein, cell, or other biological recognition element recognizes a certain analysis and transforms the biological signal into an identifying signal. A particular kind of biosensor is a peptide-based electrochemical biosensor, which recognizes target proteins utilizing certain peptide sequences with high affinity and selectivity. The aptamer biosensor is another form of biosensor utilized for protein detection. In several applications, aptamers, which are biological recognition components, can be used in place of antibodies. Another form of biosensor used to detect proteins is CRISPR/Cas-based technology (Table 3).

Table 3. Characteristics of nanowires for protein detection.

Materials	Mechanism	Target	Concentration Range	Limit of Detection	Ref.
Silicon-on-insulator (SOI)-NWs	A field-effect transistor (FET)	CA 125	10^{-15}–10^{-16} M	2.2×10^{-16} M	[55]
SiNW FET	FET	Cardiac Troponin I	0.002–0.01 ng/mL	0.002 ng/mL	[56]
ZnO NWs	Fiber-optic-based localized surface plasmon resonance (FO-LSPR)	prostate-specific antigen (PSA)	5–200 pg/mL	0.51 pg/mL	[57]
(N, S-GQDs@Au-PANI) NWs	Impedimetric immunosensor	Carcinoembryonic antigen	0.5–1000 ng mL^{-1}	0.01 ng mL^{-1}	[58]
ZnO NWs integrated inside microfluidic chips	fluorescence detection	α-fetoprotein (AFP)	1 pg/mL–1 μg/mL	1 pg/mL	[59]
Semiconductor NWs	Epifluorescence microscopy	Protein Concentration	0.25–0.00008 w%	0.00008 w%	[60]
Paper-Based Zinc Oxide NWs	Fluorescence signals	Cardiac Biomarkers of acute myocardial infarction (AMI)	1.00–7.94 ng/mL	1.00 ng/mL	[61]

Awatef reported developing a novel aptasensing substrate powered by SERS for the highly accurate and focused detection of prostate-specific antigen (PSA). Vertically aligned silicon nanowires (SiNWs) coated with silver nanoparticles (AgNPs) make up the transducing SERS substrate (Figure 9). The aptamer is immobilized using thiol chemistry and the Raman signal is enhanced by the silver nanoparticles. Only if the aptamer is present on the surface of SiNWs does the presence of PSA cause the emergence of amide bond vibration modes. The platform is sensitive, specific, and selective to PSA in a broad concentration range from 0.1 to 20 g·L^{-1} with a detection limit of 0.1 g·L^{-1}, which includes the blood serum range of both healthy participants and ill patients [56].

Kim et al. have researched sensors for localized surface plasmon resonance based on fiber optics and featuring 3D nanomaterials [57]. These sensors were designed for very sensitive plasmonic biosensing employing ZnO nanowires and AuNPs. The following features of the biosensor development stand out: (1) an expanded sensing area; (2) the influence of nanowires in trapping light; and (3) a straightforward optical system from the optical fiber. The hydrothermal fabrication of ZnO nanowires on the cross-section of fibers and AuNPs on the NWs was used to create the 3D nanomaterials. The suggested sensor produced a constant value in response to variations in the refractive index. Compared to 2D FO-LSPR sensors where a monolayer of AuNPs is attached to optical fiber, the 3D FO-LSPR sensor showed a 171% increase in the localized surface plasmon resonance response for bulk changes in refractive index. Additionally, the limits of detection for the prostate-specific antigen, a helpful biomarker for the diagnosis of prostate cancer, were 2.06 and 0.51 pg/mL, correspondingly, using 2D and 3D FO-LSPR biosensors (Figure 10).
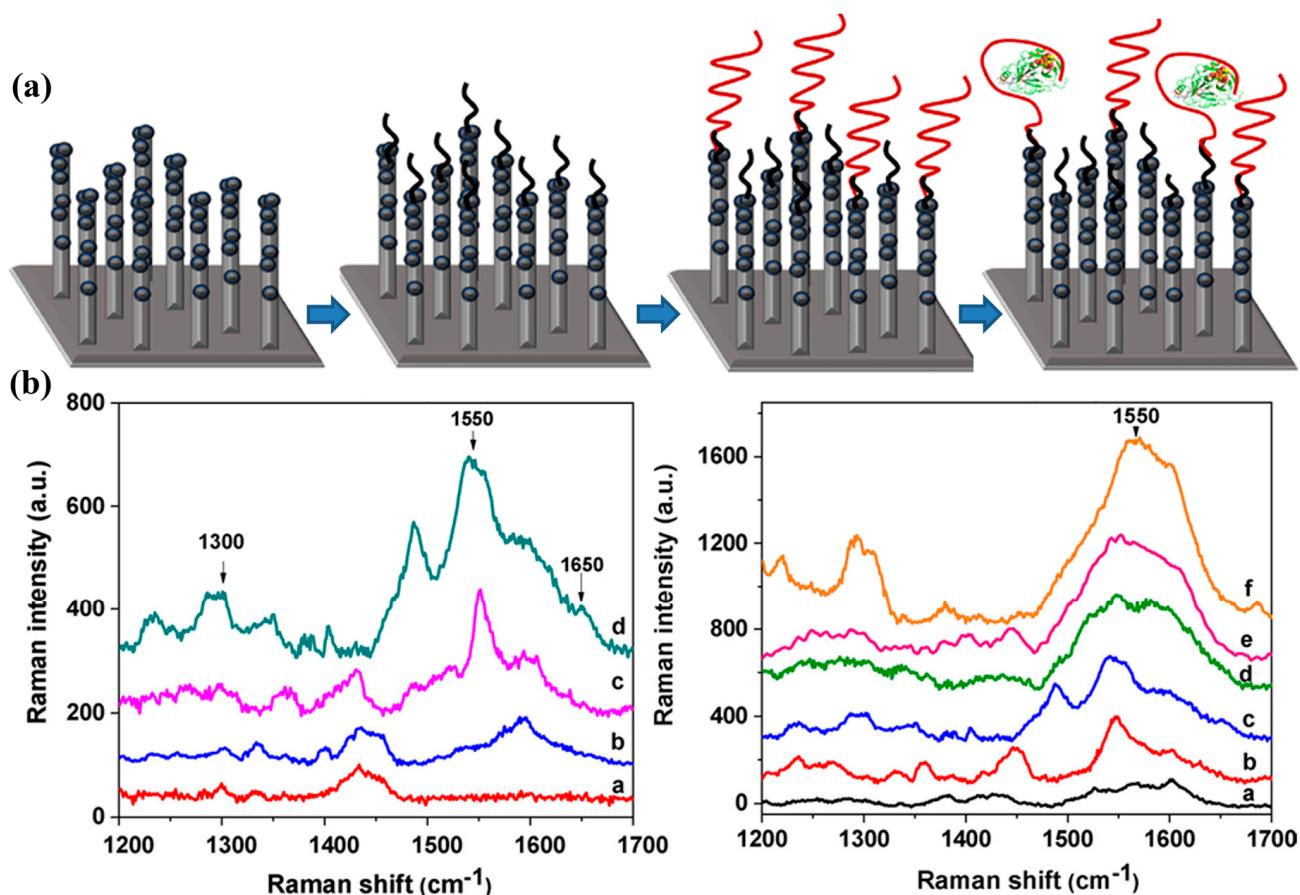
Figure 9. (**a**) A schematic depiction of the bioplatform's functionality and step-by-step assembly; (**b**) Raman spectra of MCH/AgNPs/SiNWs, PSA (1 g·L^{-1})/anti−PSA/MCH/AgNPs/SiNWs for various incubation times; 4 h (a), 8 h (b), 12 h (c), and 16 h (d) of the SERS substrate (MCH/AgNPs/SiNWs) in aptamer solutions. SERS spectra of anti−PSA/AgNP/SiNWs from the aptasensing system taken before (a) and after incubation in various PSA solutions at concentrations of 0.1 g·L^{-1} (b), 1 g·L^{-1} (c), 5 g·L^{-1} (d), 10 g·L^{-1} (e), and 20 g·L^{-1} (f) [56]. Copyright 2021 Elsevier.

To identify carcinoembryonic antigen quantitatively, N, S-graphene quantum dots@Au-polyaniline (N, S-GQDs@Au-PANI NWs) were synthesized (CEA). Simple interfacial polymerization and hydrothermal pyrolysis were used to create the N, S-GQDs, and Au-PANI, correspondingly (Figure 11). A bifunctional probe to measure an increase in electrochemical activity and attaching anti-CEA, 2–9 nm N, S-GQDs is designed by Au–PANI NWs (30–50 nm) through linkage of Au–thiol. The initiation of CEA antibody-antigen biomedical applications after the addition of CEA dramatically increases the charge transfer resistance, which is a highly reliable and label-free immunoassay technique, thus, provided for the impedimetric measurement of CEA. The N, S-GQDs@Au-PANI NWs are conductors that speed up electron transport. At the detection limit (0.01 ng mL^{-1}), the label-free immunosensor demonstrates a broad range from 0.5 to 1000 ng mL^{-1}. The immunosensor built on N, S-GQDs@Au-PANI also exhibits remarkable stability and selectivity against various cancer-causing agents and amino acids [58].
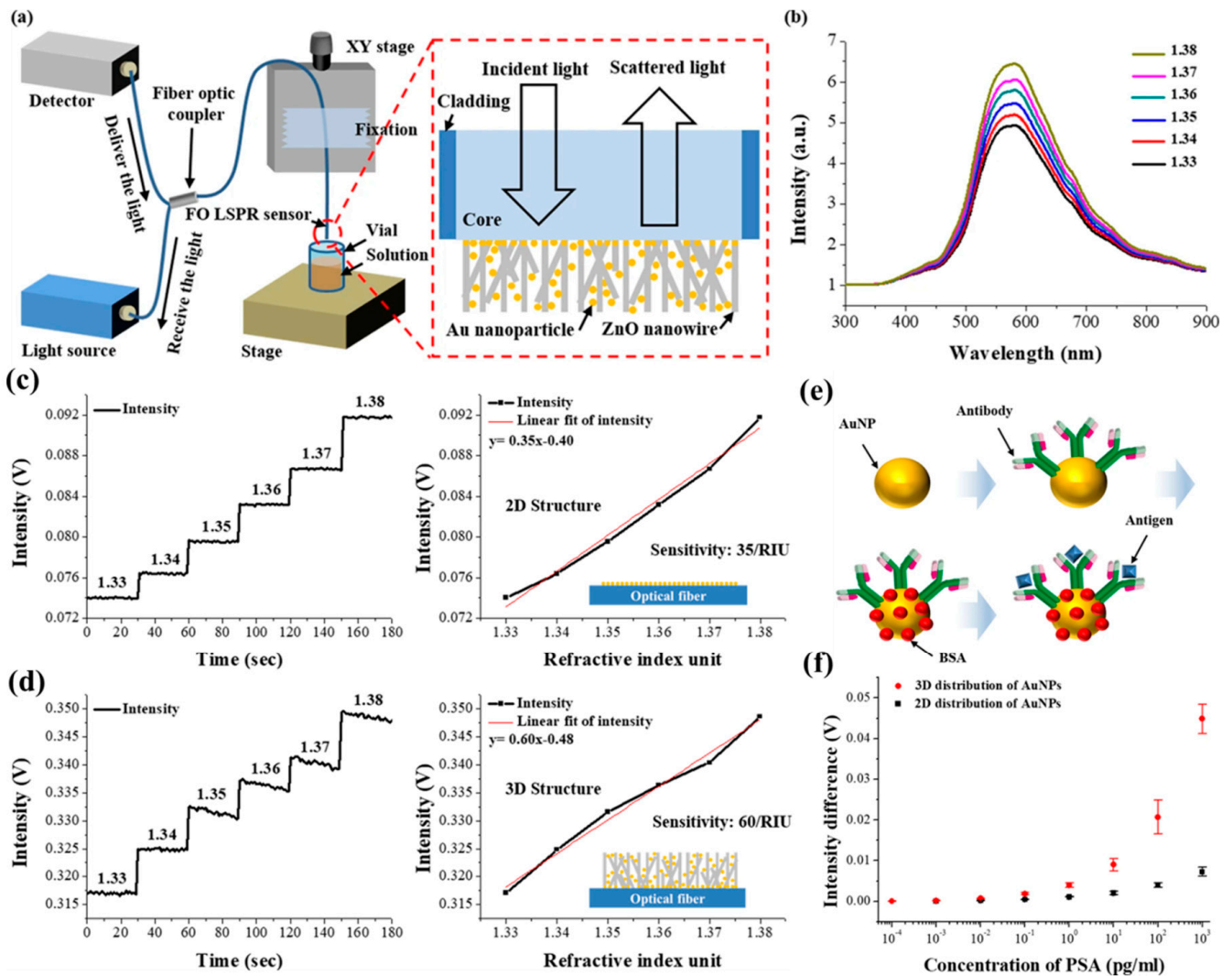
Figure 10. Localized surface plasmon resonance (LSPR) spectra measured with the suggested sensor are shown in a schematic picture together with the optical system: optical fiber−based measurement set-up (**a**) and 3D FO−LSPR sensor-measured spectra for solutions with various refractive indices (**b**). Comparison of 2D and 3D structures' refractive index sensitivities for solutions with various refractive indices; diagram showing the interaction between an antibody and an antigen and the results of measurements in 2D (**c**) and 3D (**d**) structures. (**e**) Immunoassay procedures and (**f**) the variations in intensity seen using each sensor in response to different PSA values. Reproduced with permission from [57]. Copyright 2019 Nature portfolio.
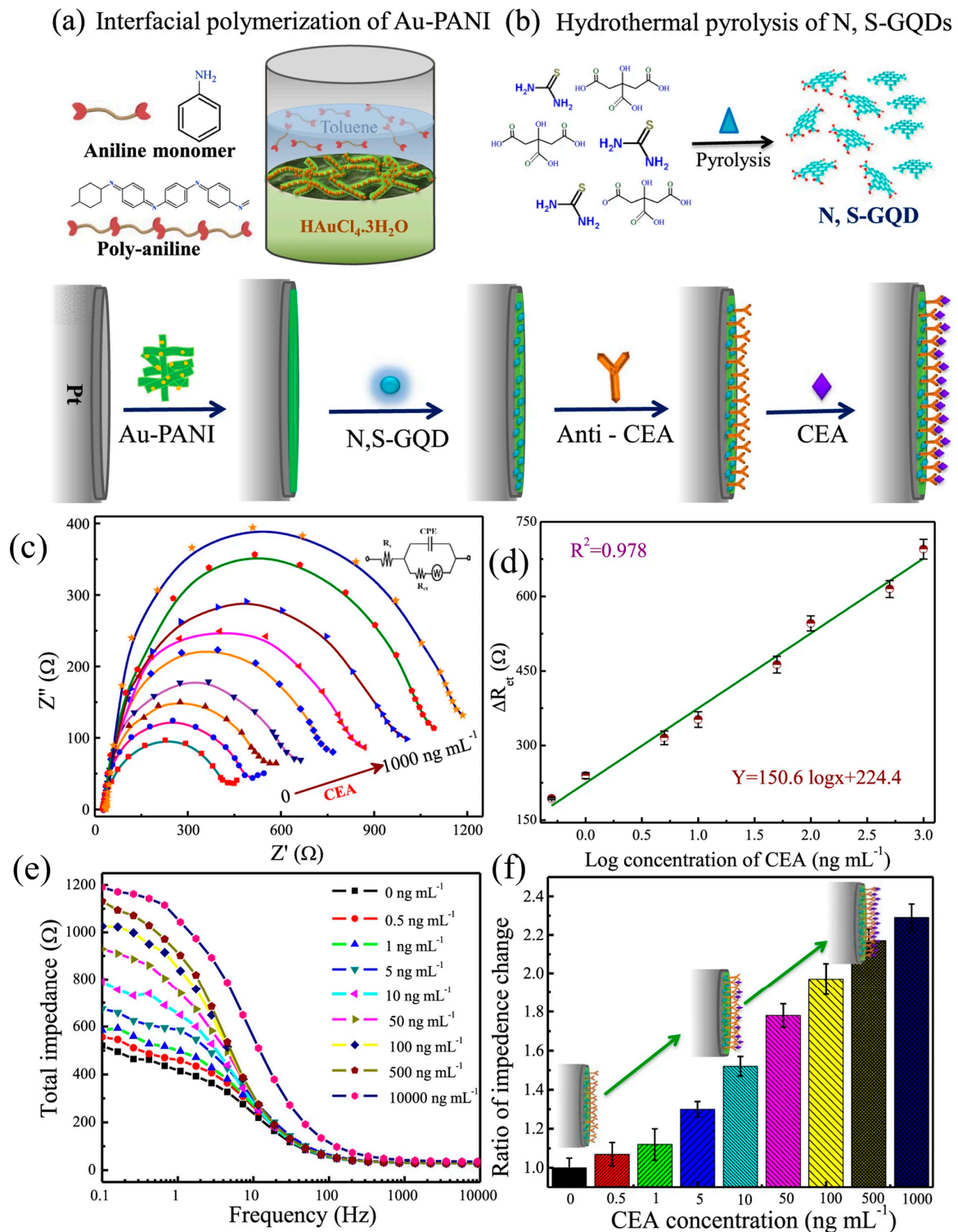
Figure 11. The schematic for the production of (**a**) electrochemically impedimetric immunosensor with no labels; (**b**) N, S−GQD hydrothermal pyrolysis, and interfacial polymerization of Au-PANI; (**c**) Nyquist plot of Pt||PANI−Au/N,S−GQDs/anti-CEA at different concentration of CEA (0–1000 ng mL^{-1}); (**d**) standard curve for the identification of CEA; (**e**) the impedance before and following exposure to different CEA concentrations; and (**f**) proportion of alteration in impedance concerning the bare Pt||PANI−Au/N,S−GQDs/anti-CEA without CEA (0.1 Hz). Reproduced with permission from [58]. Copyright 2019 Nature Portfolio.

3.4. Detection of Viruses and Bacteria

The tin-doped WO_3/In_2O_3 heterojunction NWs photoelectrode-based sensitive DNA sensor for detection of hepatitis B virus relies on laser amplification. The present COVID-19 pandemic serves as an example of how the spread of viruses and bacteria has put the world's biosecurity at risk. Disease prevention and control have historically depended heavily on the early detection of bacterial and viral illnesses. Surface-enhanced Raman scattering (SERS), surface plasmon resonance, surface-enhanced fluorescence, and surface-enhanced infrared absorption spectroscopy are some examples of plasmonic phenomena that can be used to identify viruses. This finding and evaluation will help the audience accelerate the study and creation of a novel class of adaptable bacterium and virus biosensors (Table 4).

Table 4. Characteristics of NWs for virus and bacteria detection.

Materials	Mechanism	Target	Concentration Range	Limit of Detection	Ref.
Tin-doped WO_3/In_2O_3 NWs	Electrochemical impedance spectra (EIS)	Hepatitis B virus (HBV)	0.1 pM–10 μM	1 fM	[62]
Te-doped ZnO NWs	(EIS)	HBV DNA	1 pM to 1 μM	0.1 pM	[63]
AgNWs	THz plasmonic sensors	PRD1	3.4–6.7 FOM	3.4 FOM	[64]
Porous silicon nanowire	Impedance	Influenza viruses	1000–100 TCID50	100 TCID50	[65]
Silicon nanowire (SiNW)	RT-PCR	Dengue serotype 2	10–100 fM	10 fM	[66]
Nanowire Aptamer	Gas Plasma-Treated Surface	Hepatitis C virus	2.0×10^{-15}–10^{-17} M	10^{-17} M	[67]
ZnO nanowire	Fluorescent immunoassay (FIA)	SARS-CoV-2	0 to 1500 a.u.	5 μg mL^{-1}	[68]
Gold-Decorated Silicon Nanowire	Surface-Enhanced Raman	Bilirubin	10^{-8}–5×10^{-5} M	10^{-8} M	[33]
MoS$_2$ nanowires	HBV DNA FET	Hepatitis B virus	0.5 pM to 50 μM	1 fM	[69]

A sensitive electrochemical aptasensor has been developed employing nickel nanowires (NiNWs) modified with antibodies for target separation and impedance amplification and an aptamer-coated gold interdigitated microelectrode for target capture and impedance measurement. Streptavidin was electrostatically attracted to the interdigitated microelectrode and then bound to streptavidin–biotin to create the biotinylated aptamers against Salmonella typhimurium. Then, the aptamer-bacteria-NiNW complexes were formed by incubating the bacteria NiNW complexes on the microelectrode after the target Salmonella cells had been magnetically separated and concentrated using the NiNWs modified with the anti-Salmonella typhimurium antibodies. The improved impedance change in the microelectrode was monitored and used to calculate the quantity of target bacteria after an external arc magnetic field was created and used to regulate the NiNWs to construct conductive NiNW bridges across the microelectrode. With a detection limit of 80 CFU/mL, this electrochemical aptasensor was able to quantitatively detect Salmonella with a range of 102 to 106 CFU/mL in 2 h. For the samples of drugged chicken, the average recovery was 103.2% (Figure 12).
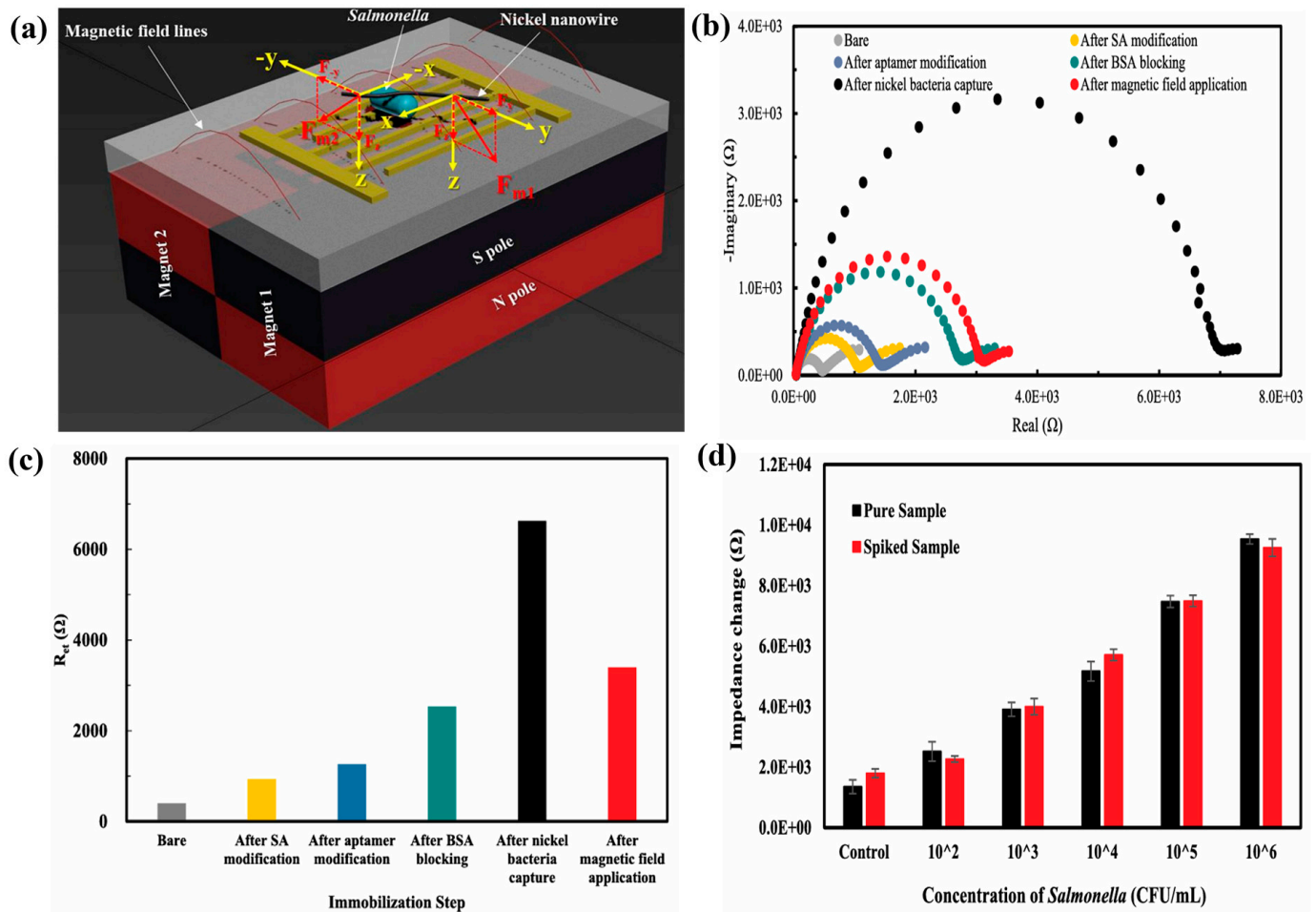
Figure 12. (**a**) The force analysis schematic for the NiNW in the magnetic field and (**b**) Streptavidin, biotinylated aptamers, BSA, and nickel bacteria at a concentration of 105 CFU/mL on the surface of the microelectrode and the application of the arc magnetic field were successively modified. The Nyquist plots after these modifications: (**c**) the change in the electron transfer resistance and (**d**) the detection of Salmonella in chicken carcass using this aptasensor (N = 3). Reproduced with permission from [62]. Copyright 2020 Elsevier.

On a microplate (MP), a ZnO NWs is developed using a hydrothermal synthesis procedure. This plate is used as a fluorescence immunoassay to find antibodies that are specific for SARS-CoV-2 NP. It is coated with SARS-CoV-2. In comparison to the bare MP, the ZnO-NW MP binds SARS-CoV-2 NP tagged to histidine at higher concentrations (up to 5 g mL^{-1}) and without any surface modification. When compared to a commercial immunoassay, an innovative serological test using the ZnO-NW MP is more sensitive, allowing for the early identification of anti-SARS-CoV-2 NP IgG antibodies in COVID-19 patients who are asymptomatic (Figure 13). This is the first assay to identify early SARS-CoV-2 antibody reactions among asymptomatic patients [68].
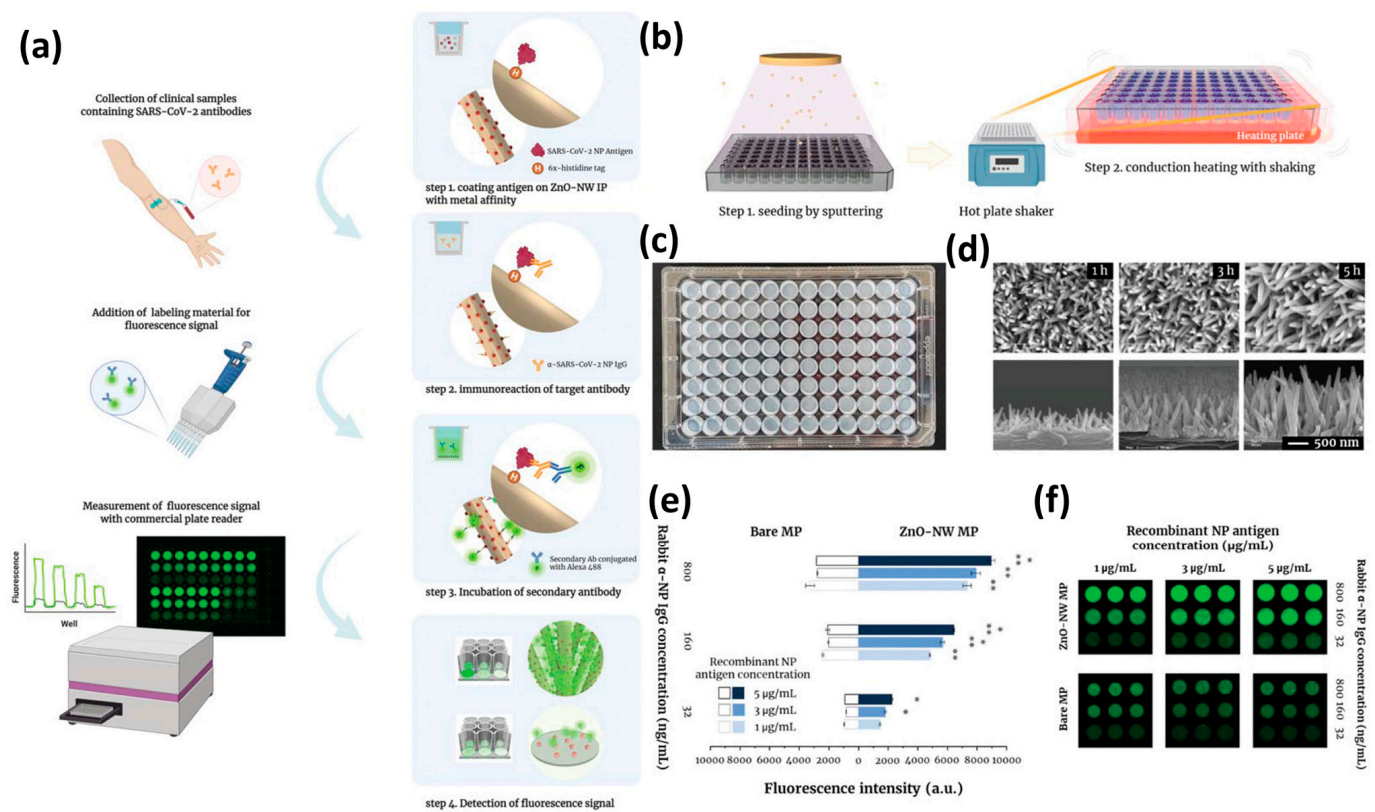
Figure 13. (**a**) Schematic depiction of the SARS-CoV-2 antibody detection procedure employing the ZnO-NW MP. Four steps make up the ZnO-NW MP-based method for detecting SARS-CoV-2 antibody responses in COVID-19 patients; (**b**) Graphic depiction of the modified ZnO-NW produced using a hydrothermal process, which involves sputtering as a seeding technique, shaking the ZnO-NW precursor solution during conduction heating, and then developing the material; (**c**) Growth of ZnO-NW MP produced using polystyrene microplate; (**d**) SEM pictures of ZnO-NWs were synthesized in a microplate for 1, 3, and 5 h. SARS-CoV-2 NP antigen is introduced to the ZnO-NW MP's surface, and anti-SARS-CoV-2 NP IgG antibodies are found there; (**e**) Both the ZnO-NW MP and the MP were coated with SARS-CoV-2 NP antigen (1, 3, 5 g mL^{-1}) employing anti-human IgG coupled to Alexa 488 to measure the fluorescence intensity and image. * $p < 0.01$ versus NP antigen at 1 μg/mL and the same antibody concentration, ** $p < 0.01$ versus anti-NP IgG at 32 ng mL^{-1} and the same antigen concentration; and (**f**) the bound rabbit anti-SARS-CoV-2 NP IgG polyclonal antibody (32, 160, 800 ng m L^{-1}). Reproduced with permission from [70]. Copyright 2022 Wiley.

As hemoglobin breaks down, bilirubin (BR), a byproduct that might signal liver problems and cause jaundice. When neonates' unconjugated BR concentrations rise quickly to fatal levels, it can result in brain damage (Figure 14). For sensitive label-free BR detection, Anna et al. suggest a novel technique for fabricating a SERS-active substrate using gold-decorated silicon NWs (Au@SiNWs). To create SiNWs, crystalline silicon wafers were chemically etched with the help of gold before being further embellished with gold. The model analyte 4-mercaptopyridine has a low detection limit down to a concentration of 10^{-8} M. Amino groups were added to the surface of the SiNWs to facilitate effective BR adsorption and SERS detection. The required sensitivity for clinical applications, 5×10^{-5} M for BR adsorption, was used to verify the signal stability for 7 days [33].
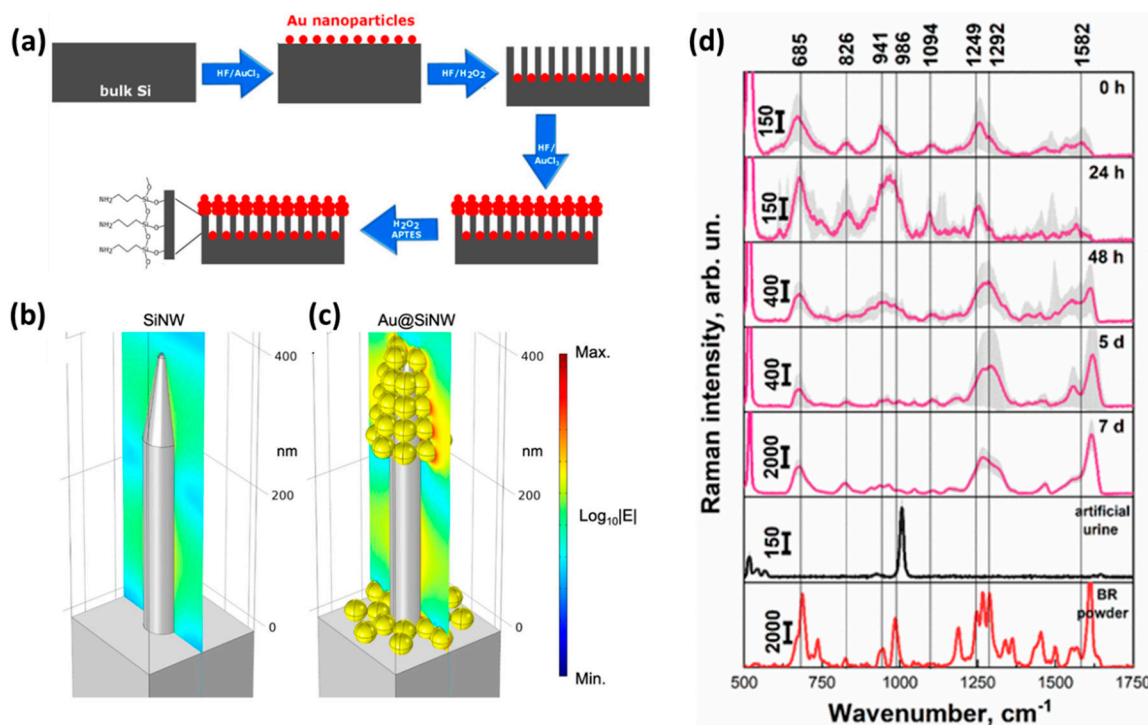
Figure 14. (**a**) A schematic illustration of how Au@SiNWs substrates are developed and then have their surfaces modified. Distribution of the tested electric field when it is ordinarily incident on either (**b**) a periodic SiNW or (**c**) a periodic Au@SiNW substrate. The color represents the log10(E) value, where E is the vector of the electric field. For = 633 nm, calculations are performed. (**d**) BR powder Raman spectrum, average SERS spectrum of artificial urine, at a concentration of 5×10^{-5} M in artificial urine for Au@SiNWs at various times (0−7 days) after BR adsorption. The standard deviations derived from spectra are indicated by the shading of gray in the average spectra. Reproduced with permission from [33]. Copyright 2021 ACS.

4. Conclusions and Perspective

In the disciplines of engineering and technology, biomedicine, ecotoxicology, toxicology, food safety monitoring, disease progression, and medication delivery, biosensors have a wide range of applications. In this review, we have covered how to construct nanowires that can be used as biosensors for various pathogens and bacteria, protease [71], DNA [72] and RNA [73], neurotransmitters, and molecular molecules. The use of nanowires in biosensors has led to a dramatic increase in biosensing technology during the past ten years [74]. This is due to the utilization of new biorecognition components and transducers, advancements in the production, design, and miniaturization of nanostructured devices at the micron scale, and novel methods for the creation of nanowires [75]. The use of nanowires has increased the sensing technology's adaptability, durability, and dynamic nature [76]. By utilizing several nanowires with various properties within biosensors, the transduction process has been greatly improved (such as increased sensitivity, faster detection, shorter response time, and reproducibility).

The nanowire sensor will depend on how much ahead it is in comparison to the present gold standards, such as ELISA and PCR, in terms of ease of use, specificity, sensitivity, and dependability. Despite having incredibly high sensitivity in comparison to other approaches, in vivo environments in particular, its analytical signal strength is still too low to be corrupted by significant background noise. This increased sensitivity issue as well as simpler fabrication processing problems may be solved by advancements in receptor binding techniques [77]. Additionally, the reduced cost of commercially available items is made possible by the present top-down production processes' greater yield ratio.

To improve device performance and detection, several nanowires-related challenges need to be resolved. The problems with these biosensors include (i) the toxicity, which varies depending on the physical characteristics of the material type, (ii) the production of nanostructures, and (iii) the sustainability of nanostructures in sensor applications, which has not been properly examined. The majority of biosensors used in biomedical applications need a sizable sample to identify an object, which could result in false-positive or false-negative results. On a global scale, only a few biosensors have achieved commercial success. More study is needed in this area, and we anticipate that companies will soon translate the current academic research into prototypes that are practical from a commercial standpoint. Particularly, it is anticipated that nanowires would lead to the creation of potential wearable biosensors.

Author Contributions: V.A.T.: writing—original draft, methodology, investigation, software, writing—review and editing, funding acquisition, project administration, supervision. G.N.L.V.: methodology, software, resources. T.-T.T.V.: writing—original draft, methodology, investigation, writing. V.D.D.: methodology, software, resources. V.V.: investigation, software, methodology. V.T.L.: methodology, investigation, software, resources. All authors have read and agreed to the published version of the manuscript.

Data Availability Statement: All the data are contained within the manuscript.

Conflicts of Interest: The authors declare no conflict of interest.

References

1. Shao, Q.; Lu, K.; Huang, X. Platinum Group Nanowires for Efficient Electrocatalysis. *Small Methods* **2019**, *3*, 1800545. [CrossRef]
2. Xu, Z.; He, X.; Liang, M.; Sun, L.; Li, D.; Xie, K.; Liao, L. Catalytic reduction of 4-nitrophenol over graphene supported Cu@Ni bimetallic nanowires. *Mater. Chem. Phys.* **2019**, *227*, 64–71. [CrossRef]
3. Karabiberoğlu, Ş.U.; Koçak, Ç.C.; Dursun, Z. Electrochemical Determination of Dicofol at Nickel Nanowire Modified Poly(p-aminophenol) Film Electrode. *Electroanalysis* **2019**, *31*, 1304–1310. [CrossRef]
4. Kim, M.J.; Cruz, M.A.; Yang, F.; Wiley, B.J. Accelerating electrochemistry with metal nanowires. *Curr. Opin. Electro-Chem.* **2019**, *16*, 19–27. [CrossRef]
5. Li, X.; Mo, J.; Fang, J.; Xu, D.; Yang, C.; Zhang, M.; Li, H.; Xie, X.; Hu, N.; Liu, F. Vertical nanowire array-based biosensors: Device design strategies and biomedical applications. *J. Mater. Chem. B* **2020**, *8*, 7609–7632. [CrossRef] [PubMed]
6. Tran, V.A.; Tran, N.T.; Doan, V.D.; Nguyen, T.-Q.; Thi, H.H.P.; Vo, G.N.L. Application Prospects of MXenes Materials Modifications for Sensors. *Micromachines* **2023**, *14*, 247. [CrossRef]
7. Tran, V.A.; Doan, V.D.; Le, V.T.; Nguyen, T.-Q.; Don, T.N.; Vien, V.; Luan, N.T.; Vo, G.N.L. Metal–Organic Frameworks-Derived Material for Electrochemical Biosensors: Recent Applications and Prospects. *Ind. Eng. Chem. Res.* **2023**, *62*, 4738–4753. [CrossRef]
8. Gupta, R.K. *Nanowires: Applications, Chemistry, Materials, and Technologies*; CRC Press: Boca Raton, FL, USA, 2023.
9. Adam, T.; Dhahi, T.S.; Gopinath, S.C.B.; Hashim, U. Novel Approaches in Fabrication and Integration of Nanowire for Micro/Nano Systems. *Crit. Rev. Anal. Chem.* **2022**, *52*, 1913–1929. [CrossRef]
10. Liu, R.; Lee, J.; Tchoe, Y.; Pre, D.; Bourhis, A.M.; D'Antonio-Chronowska, A.; Robin, G.; Lee, S.H.; Ro, Y.G.; Vatsyayan, R.; et al. Ultra-Sharp Nanowire Arrays Natively Permeate, Record, and Stimulate Intracellular Activity in Neuronal and Cardiac Networks. *Adv. Funct. Mater.* **2022**, *32*, 2108378. [CrossRef]
11. Shi, J.; Sun, C.; Liang, E.; Tian, B. Semiconductor Nanowire-Based Cellular and Subcellular Interfaces. *Adv. Funct. Mater.* **2022**, *32*, 2107997. [CrossRef]
12. Tian, B.; Lieber, C.M. Nanowired Bioelectric Interfaces. *Chem. Rev.* **2019**, *119*, 9136–9152. [CrossRef] [PubMed]
13. Meng, J.; Li, Z. Schottky-Contacted Nanowire Sensors. *Adv. Mater.* **2020**, *32*, 2000130. [CrossRef] [PubMed]
14. Smith, A.F.; Liu, X.; Woodard, T.L.; Fu, T.; Emrick, T.; Jiménez, J.M.; Lovley, D.R.; Yao, J. Bioelectronic protein nanowire sensors for ammonia detection. *Nano Res.* **2020**, *13*, 1479–1484. [CrossRef]
15. Bagchi, B.; Fernandez, C.S.; Bhatti, M.; Ciric, L.; Lovat, L.; Tiwari, M.K. Copper nanowire embedded hypromellose: An antibacterial nanocomposite film. *J. Colloid Interface Sci.* **2022**, *608*, 30–39. [CrossRef]
16. Fanton, L.; Loria, F.; Amores, M.; Pazos, M.R.; Adán, C.; García-Muñoz, R.A.; Marugán, J. Proliferation of osteoblast precursor cells on the surface of TiO$_2$ nanowires anodically grown on a β-type biomedical titanium alloy. *Sci. Rep.* **2022**, *12*, 7895. [CrossRef]
17. Wang, H.; Tang, M.; Shi, F.; Ding, R.; Wang, L.; Wu, J.; Li, X.; Liu, Z.; Lv, B. Amorphous Cr$_2$WO$_6$-Modified WO$_3$ Nanowires with a Large Specific Surface Area and Rich Lewis Acid Sites: A Highly Efficient Catalyst for Oxidative Desulfurization. *ACS Appl. Mater. Interfaces* **2020**, *12*, 38140–38152. [CrossRef]

18. Liu, D.; Liu, Y.; Liu, X.; Xu, C.; Zhu, J.; Chen, H. Growth of uniform CuCo$_2$O$_4$ porous nanosheets and nanowires for high-performance hybrid supercapacitors. *J. Energy Storage* **2022**, *52*, 105048. [CrossRef]

19. Prameswati, A.; Han, J.W.; Kim, J.H.; Wibowo, A.F.; Entifar, S.A.N.; Park, J.; Lee, J.; Kim, S.; Lim, D.C.; Moon, M.-W.; et al. Highly stretchable and mechanically robust silver nanowires on surface-functionalized wavy elastomers for wearable healthcare electronics. *Org. Electron.* **2022**, *108*, 106584. [CrossRef]

20. Jung, J.; Shin, S.; Kim, Y.T. Dry electrode made from carbon nanotubes for continuous recording of bio-signals. *Microelectron. Eng.* **2019**, *203–204*, 25–30. [CrossRef]

21. Khanna, S.; Paneliya, S.; Makani, N.H.; Mukhopadhyay, I.; Banerjee, R. Controlled restructuring of bidisperse silica nanospheres for size-selective nanowire growth. *Mater. Chem. Phys.* **2021**, *273*, 125063. [CrossRef]

22. Chang, T.-Y.; Kim, H.; Zutter, B.T.; Lee, W.-J.; Regan, B.C.; Huffaker, D.L. Orientation-Controlled Selective-Area Epitaxy of III–V Nanowires on (001) Silicon for Silicon Photonics. *Adv. Funct. Mater.* **2020**, *30*, 2002220. [CrossRef]

23. Tran, V.A.; Le, V.T.; Doan, V.D.; Vo, G.N.L. Utilization of Functionalized Metal–Organic Framework Nanoparticle as Targeted Drug Delivery System for Cancer Therapy. *Pharmaceutics* **2023**, *15*, 931. [CrossRef] [PubMed]

24. Tran, V.A.; Van Vo, G.; Tan, M.A.; Park, J.-S.; An, S.S.A.; Lee, S.-W. Dual Stimuli-Responsive Multifunctional Silicon Nanocarriers for Specifically Targeting Mitochondria in Human Cancer Cells. *Pharmaceutics* **2022**, *14*, 858. [CrossRef]

25. Tran, V.A.; Lee, S.-W. pH-triggered degradation and release of doxorubicin from zeolitic imidazolate framework-8 (ZIF8) decorated with polyacrylic acid. *RSC Adv.* **2021**, *11*, 9222–9234. [CrossRef]

26. Tran, V.A.; Vo, V.G.; Shim, K.; Lee, S.-W.; A An, S.S. Multimodal Mesoporous Silica Nanocarriers for Dual Stimuli-Responsive Drug Release and Excellent Photothermal Ablation of Cancer Cells. *Int. J. Nanomed.* **2020**, *15*, 7667–7685. [CrossRef] [PubMed]

27. Tran, A.-V.; Shim, K.; Thi, T.-T.V.; Kook, J.-K.; An, S.S.A.; Lee, S.-W. Targeted and controlled drug delivery by multifunctional mesoporous silica nanoparticles with internal fluorescent conjugates and external polydopamine and graphene oxide layers. *Acta Biomater.* **2018**, *74*, 397–413. [CrossRef] [PubMed]

28. Tran, V.A.; Lee, S.-W. A prominent anchoring effect on the kinetic control of drug release from mesoporous silica nanoparticles (MSNs). *J. Colloid Interface Sci.* **2018**, *510*, 345–356. [CrossRef]

29. Takahashi, H.; Baba, Y.; Yasui, T. Oxide nanowire microfluidics addressing previously-unattainable analytical methods for bi-omolecules towards liquid biopsy. *Chem. Commun.* **2021**, *57*, 13234–13245. [CrossRef]

30. Kim, K.; Park, C.; Kwon, D.; Kim, D.; Meyyappan, M.; Jeon, S.; Lee, J.-S. Silicon nanowire biosensors for detection of cardiac troponin I (cTnI) with high sensitivity. *Biosens. Bioelectron.* **2016**, *77*, 695–701. [CrossRef]

31. Zhang, H.; Kikuchi, N.; Ohshima, N.; Kajisa, T.; Sakata, T.; Izumi, T.; Sone, H. Design and Fabrication of Silicon Nanowire-Based Biosensors with Integration of Critical Factors: Toward Ultrasensitive Specific Detection of Biomolecules. *ACS Appl. Mater. Interfaces* **2020**, *12*, 51808–51819. [CrossRef]

32. Kim, N.; Han, K.; Su, P.-C.; Kim, I.; Yoon, Y.-J. A rotationally focused flow (RFF) microfluidic biosensor by density difference for early-stage detectable diagnosis. *Sci. Rep.* **2021**, *11*, 9277. [CrossRef] [PubMed]

33. Kartashova, A.D.; Gonchar, K.A.; Chermoshentsev, D.A.; Alekseeva, E.A.; Gongalsky, M.B.; Bozhev, I.V.; Eliseev, A.A.; Dy-akov, S.A.; Samsonova, J.V.; Osminkina, L.A. Surface-Enhanced Raman Scattering-Active Gold-Decorated Silicon Nanowire Sub-strates for Label-Free Detection of Bilirubin. *ACS Biomater. Sci. Eng.* **2022**, *8*, 4175–4184. [CrossRef] [PubMed]

34. Wang, J.; Hui, N. Electrochemical functionalization of polypyrrole nanowires for the development of ultrasensitive biosensors for detecting microRNA. *Sens. Actuators B Chem.* **2019**, *281*, 478–485. [CrossRef]

35. Takahashi, H.; Yasui, T.; Klamchuen, A.; Khemasiri, N.; Wuthikhun, T.; Paisrisarn, P.; Shinjo, K.; Kitano, Y.; Aoki, K.; Natsume, A.; et al. Annealed ZnO/Al$_2$O$_3$ Core-Shell Nanowire as a Platform to Capture RNA in Blood Plasma. *Nanomaterials* **2021**, *11*, 1768. [CrossRef]

36. Li, Z.; Liu, C.; Sarpong, V.; Gu, Z. Multisegment nanowire/nanoparticle hybrid arrays as electrochemical biosensors for simul-taneous detection of antibiotics. *Biosens. Bioelectron.* **2019**, *126*, 632–639. [CrossRef] [PubMed]

37. Hou, J.; Jia, P.; Yang, K.; Bu, T.; Sun, X.; Wang, L. Facile preparation of Ru@V$_2$O$_4$ nanowires exhibiting excellent tetra-enzyme mimetic activities for sensitive colorimetric H$_2$O$_2$ and cysteine sensing. *Sens. Actuators B Chem.* **2021**, *344*, 130266. [CrossRef]

38. Naresh, V.; Lee, N. A Review on Biosensors and Recent Development of Nanostructured Materials-Enabled Biosensors. *Sensors* **2021**, *21*, 1109. [CrossRef]

39. Ambhorkar, P.; Wang, Z.; Ko, H.; Lee, S.; Koo, K.-I.; Kim, K.; Cho, D.-I.D. Nanowire-Based Biosensors: From Growth to Applications. *Micromachines* **2018**, *9*, 679. [CrossRef]

40. Lee, J.-H.; Chae, E.-J.; Park, S.-J.; Choi, J.-W. Label-free detection of γ-aminobutyric acid based on silicon nanowire biosensor. *Nano Converg.* **2019**, *6*, 13. [CrossRef]

41. Luo, J.; Cui, J.; Wang, Y.; Yu, D.; Qin, Y.; Zheng, H.; Shu, X.; Tan, H.H.; Zhang, Y.; Wu, Y. Metal-organic framework-derived porous Cu$_2$O/Cu@C core-shell nanowires and their application in uric acid biosensor. *Appl. Surf. Sci.* **2020**, *506*, 144662. [CrossRef]

42. Yan, B.; Zhuang, Y.; Jiang, Y.; Xu, W.; Chen, Y.; Tu, J.; Wang, X.; Wu, Q. Enhanced photoeletrochemical biosensing performance from rutile nanorod/anatase nanowire junction array. *Appl. Surf. Sci.* **2018**, *458*, 382–388. [CrossRef]

43. Mariyappan, V.; Jeyapragasam, T.; Chen, S.-M.; Murugan, K. Mo-W-O nanowire intercalated graphene aerogel nanocomposite for the simultaneous determination of dopamine and tyrosine in human urine and blood serum sample. *J. Electroanal. Chem.* **2021**, *895*, 115391. [CrossRef]

44. Guo, X.; Wu, J.; Xia, L.; Xiang, M.; Qu, F.; Li, J. CuO/Cu2O nanowire array photoelectrochemical biosensor for ultrasensitive detection of tyrosinase. *Sci. China Chem.* **2020**, *63*, 1012–1018. [CrossRef]
45. Russell, C.; Welch, K.; Jarvius, J.; Cai, Y.; Brucas, R.; Nikolajeff, F.; Svedlindh, P.; Nilsson, M. Gold Nanowire Based Electrical DNA Detection Using Rolling Circle Amplification. *ACS Nano* **2014**, *8*, 1147–1153. [CrossRef]
46. Zhang, J.; Han, D.; Yang, R.; Ji, Y.; Liu, J.; Yu, X. Electrochemical detection of DNA hybridization based on three-dimensional ZnO nanowires/graphite hybrid microfiber structure. *Bioelectrochemistry* **2019**, *128*, 126–132. [CrossRef] [PubMed]
47. Barozzi, M.; Manicardi, A.; Vannucci, A.; Candiani, A.; Sozzi, M.; Konstantaki, M.; Pissadakis, S.; Corradini, R.; Selleri, S.; Cucinotta, A. Optical Fiber Sensors for Label-Free DNA Detection. *J. Light. Technol.* **2017**, *35*, 3461–3472. [CrossRef]
48. Tai, Y.-H.; Fu, P.-H.; Lee, K.-L.; Wei, P.-K. Spectral Imaging Analysis for Ultrasensitive Biomolecular Detection Using Gold-Capped Nanowire Arrays. *Sensors* **2018**, *18*, 2181. [CrossRef]
49. Shariati, M. The field effect transistor DNA biosensor based on ITO nanowires in label-free hepatitis B virus detecting compatible with CMOS technology. *Biosens. Bioelectron.* **2018**, *105*, 58–64. [CrossRef]
50. Chou, W.-C.; Hu, W.-P.; Yang, Y.-S.; Chan, H.W.-H.; Chen, W.-Y. Neutralized chimeric DNA probe for the improvement of GC-rich RNA detection specificity on the nanowire field-effect transistor. *Sci. Rep.* **2019**, *9*, 11056. [CrossRef]
51. Ding, W.; Song, C.; Li, T.; Ma, H.; Yao, Y.; Yao, C. TiO$_2$ nanowires as an effective sensing platform for rapid fluorescence detection of single-stranded DNA and double-stranded DNA. *Talanta* **2019**, *199*, 442–448. [CrossRef]
52. Ivanov, Y.D.; Malsagova, K.A.; Popov, V.P.; Kupriyanov, I.N.; Pleshakova, T.O.; Galiullin, R.A.; Ziborov, V.S.; Dolgoborodov, A.Y.; Petrov, O.F.; Miakonkikh, A.V.; et al. Micro-Raman Characterization of Structural Features of High-k Stack Layer of SOI Nanowire Chip, Designed to Detect Circular RNA Associated with the Development of Glioma. *Molecules* **2021**, *26*, 3715. [CrossRef] [PubMed]
53. Vu, C.-A.; Lai, H.-Y.; Chang, C.-Y.; Chan, H.W.-H.; Chen, W.-Y. Optimizing surface modification of silicon nanowire field-effect transistors by polyethylene glycol for MicroRNA detection. *Colloids Surf. B Biointerfaces* **2022**, *209*, 112142. [CrossRef] [PubMed]
54. Zhang, G.-J.; Luo, Z.H.H.; Huang, M.J.; Tay, G.K.I.; Lim, E.-J.A. Morpholino-functionalized silicon nanowire biosensor for sequence-specific label-free detection of DNA. *Biosens. Bioelectron.* **2010**, *25*, 2447–2453. [CrossRef]
55. Malsagova, K.A.; Pleshakova, T.O.; Galiullin, R.A.; Kozlov, A.F.; Shumov, I.D.; Popov, V.P.; Tikhonenko, F.V.; Glukhov, A.V.; Ziborov, V.S.; Petrov, O.F.; et al. Highly Sensitive Detection of CA 125 Protein with the Use of an n-Type Nanowire Biosensor. *Biosensors* **2020**, *10*, 210. [CrossRef] [PubMed]
56. Ouhibi, A.; Raouafi, A.; Lorrain, N.; Guendouz, M.; Raouafi, N.; Moadhen, A. Functionalized SERS substrate based on silicon nanowires for rapid detection of prostate specific antigen. *Sens. Actuators B Chem.* **2021**, *330*, 129352. [CrossRef]
57. Kim, H.-M.; Park, J.-H.; Lee, S.-K. Fiber optic sensor based on ZnO nanowires decorated by Au nanoparticles for improved plasmonic biosensor. *Sci. Rep.* **2019**, *9*, 15605. [CrossRef]
58. Ganganboina, A.B.; Doong, R.-A. Graphene Quantum Dots Decorated Gold-Polyaniline Nanowire for Impedimetric Detection of Carcinoembryonic Antigen. *Sci. Rep.* **2019**, *9*, 7214. [CrossRef]
59. Guo, L.; Shi, Y.; Liu, X.; Han, Z.; Zhao, Z.; Chen, Y.; Xie, W.; Li, X. Enhanced fluorescence detection of proteins using ZnO nanowires integrated inside microfluidic chips. *Biosens. Bioelectron.* **2018**, *99*, 368–374. [CrossRef]
60. Verardo, D.; Agnarsson, B.; Zhdanov, V.P.; Höök, F.; Linke, H. Single-Molecule Detection with Lightguiding Nanowires: Determination of Protein Concentration and Diffusivity in Supported Lipid Bilayers. *Nano Lett.* **2019**, *19*, 6182–6191. [CrossRef]
61. Guo, X.; Zong, L.; Jiao, Y.; Han, Y.; Zhang, X.; Xu, J.; Li, L.; Zhang, C.-W.; Liu, Z.; Ju, Q.; et al. Signal-Enhanced Detection of Multiplexed Cardiac Biomarkers by a Paper-Based Fluorogenic Immunodevice Integrated with Zinc Oxide Nanowires. *Anal. Chem.* **2019**, *91*, 9300–9307. [CrossRef]
62. Wang, L.; Huo, X.; Qi, W.; Xia, Z.; Li, Y.; Lin, J. Rapid and sensitive detection of Salmonella Typhimurium using nickel nanowire bridge for electrochemical impedance amplification. *Talanta* **2020**, *211*, 120715. [CrossRef] [PubMed]
63. Khosravi-Nejad, F.; Teimouri, M.; Marandi, S.J.; Shariati, M. The highly sensitive impedimetric biosensor in label free ap-proach for hepatitis B virus DNA detection based on tellurium doped ZnO nanowires. *Appl. Phys. A* **2019**, *125*, 616. [CrossRef]
64. Hong, J.T.; Jun, S.W.; Cha, S.H.; Park, J.Y.; Lee, S.; Shin, G.A.; Ahn, Y.H. Enhanced sensitivity in THz plasmonic sensors with silver nanowires. *Sci. Rep.* **2018**, *8*, 15536. [CrossRef] [PubMed]
65. Gongalsky, M.B.; Tsurikova, U.A.; Samsonova, J.V.; Gvindzhiliiia, G.Z.; Gonchar, K.A.; Saushkin, N.Y.; Kudryavtsev, A.A.; Kropotkina, E.A.; Gambaryan, A.S.; Osminkina, L.A. Double etched porous silicon nanowire arrays for impedance sensing of in-fluenza viruses. *Results Mater.* **2020**, *6*, 100084. [CrossRef]
66. Zhang, G.-J.; Zhang, L.; Huang, M.J.; Luo, Z.H.H.; Tay, G.K.I.; Lim, E.-J.A.; Kang, T.G.; Chen, Y. Silicon nanowire biosensor for highly sensitive and rapid detection of Dengue virus. *Sens. Actuators B Chem.* **2010**, *146*, 138–144. [CrossRef]
67. Malsagova, K.A.; Pleshakova, T.O.; Galiullin, R.A.; Shumov, I.D.; Kozlov, A.F.; Romanova, T.S.; Popov, V.P.; Glukhov, A.V.; Konev, V.A.; Archakov, A.I.; et al. Nanowire Aptamer-Sensitized Biosensor Chips with Gas Plasma-Treated Surface for the Detection of Hepatitis C Virus Core Antigen. *Coatings* **2020**, *10*, 753. [CrossRef]
68. Wasfi, A.; Awwad, F.; Gelovani, J.G.; Qamhieh, N.; Ayesh, A.I. COVID-19 Detection via Silicon Nanowire Field-Effect Transistor: Setup and Modeling of Its Function. *Nanomaterials* **2022**, *12*, 2638. [CrossRef]
69. Shariati, M.; Vaezjalali, M.; Sadeghi, M. Ultrasensitive and easily reproducible biosensor based on novel doped MoS2 nanowires field-effect transistor in label-free approach for detection of hepatitis B virus in blood serum. *Anal. Chim. Acta* **2021**, *1156*, 338360. [CrossRef]

70. Kim, J.; Lee, S.K.; Lee, J.H.; Kim, H.Y.; Kim, N.H.; Lee, C.H.; Lee, C.S.; Kim, H.G. ZnO Nanowire-Based Early Detection of SARS-CoV-2 Antibody Responses in Asymptomatic Patients with COVID-19. *Adv. Mater. Interfaces* **2022**, *9*, 2102046. [CrossRef]
71. Li, J.; He, G.; Ueno, H.; Jia, C.; Noji, H.; Qi, C.; Guo, X. Direct real-time detection of single proteins using silicon nanowire-based electrical circuits. *Nanoscale* **2016**, *8*, 16172–16176. [CrossRef]
72. Hui, N.; Sun, X.; Niu, S.; Luo, X. PEGylated Polyaniline Nanofibers: Antifouling and Conducting Biomaterial for Electrochemical DNA Sensing. *ACS Appl. Mater. Interfaces* **2017**, *9*, 2914–2923. [CrossRef] [PubMed]
73. Yang, L.; Wang, H.; Lü, H.; Hui, N. Phytic acid functionalized antifouling conducting polymer hydrogel for electrochemical detection of microRNA. *Anal. Chim. Acta* **2020**, *1124*, 104–112. [CrossRef] [PubMed]
74. Leonardi, A.A.; Sciuto, E.L.; Faro, M.J.L.; Fazio, B.; Rizzo, M.G.; Calabrese, G.; Francioso, L.; Picca, R.; Nastasi, F.; Mancuso, G.; et al. SARS-CoV-2 and omicron variant detection with a high selectivity, sensitivity, and low-cost silicon bio-nanosensor. *Nano Sel.* **2023**, *4*, 160–169. [CrossRef] [PubMed]
75. Lu, N.; Dai, P.; Gao, A.; Valiaho, J.; Kallio, P.; Wang, Y.; Li, T. Label-Free and Rapid Electrical Detection of hTSH with CMOS-Compatible Silicon Nanowire Transistor Arrays. *ACS Appl. Mater. Interfaces* **2014**, *6*, 20378–20384. [CrossRef]
76. Nick, C.; Quednau, S.; Sarwar, R.; Schlaak, H.F.; Thielemann, C. High aspect ratio gold nanopillars on microelectrodes for neural interfaces. *Microsyst. Technol.* **2014**, *20*, 1849–1857. [CrossRef]
77. Hui, N.; Sun, X.; Song, Z.; Niu, S.; Luo, X. Gold nanoparticles and polyethylene glycols functionalized conducting polyaniline nanowires for ultrasensitive and low fouling immunosensing of alpha-fetoprotein. *Biosens. Bioelectron.* **2016**, *86*, 143–149. [CrossRef]